



Article

# Investigations of the Friction Losses of Different Engine Concepts. Part 1: A Combined Approach for Applying Subassembly-Resolved Friction Loss Analysis on a Modern Passenger-Car Diesel Engine

Christoph Knauder <sup>1,\*</sup>, Hannes Allmaier <sup>1</sup> , David E. Sander <sup>1</sup> and Theodor Sams <sup>2,3</sup>

<sup>1</sup> VIRTUAL VEHICLE Research Center, Inffeldgasse 21A, 8010 Graz, Austria; Hannes.Allmaier@v2c2.at (H.A.); David.Sander@v2c2.at (D.E.S.)

<sup>2</sup> AVL List GmbH, Hans-List-Platz 1, 8020 Graz, Austria; Theodor.Sams@avl.com

<sup>3</sup> Institute of Internal Combustion Engines and Thermodynamics—Graz University of Technology, Inffeldgasse 19, 8010 Graz, Austria

\* Correspondence: christoph.knauder@v2c2.at

Received: 29 March 2019; Accepted: 17 April 2019; Published: 26 April 2019



**Abstract:** This work presents the application of a combined approach to investigate the friction losses in a modern four-cylinder passenger-car diesel engine. The approach connects the results from engine friction measurements using the indication method and the results from journal-bearing simulations. The utilization of the method enables a subassembly-resolved friction loss analysis that yields the losses of the piston group, crankshaft journal bearings, and valve train (including the timing drive and crankshaft seals). The engine and engine subassembly friction losses are investigated over the full speed and load range, covering more than 120 engine operation points at different engine media supply temperatures ranging from 70 to 110 °C. The subsequently decreasing lubricant viscosity due to higher engine media supply temperatures allow for the identification of friction reduction potentials as well as possible risks due to an onset of mixed lubrication. Furthermore, additional strip-tests have been conducted to determine the friction losses of the crankshaft radial lip seals, the timing drive, and the crankshaft journal bearings, thus enabling a verification of the calculated journal-bearing friction losses with measurement results. For the investigated diesel engine, a friction reduction potential of up to 21% could be determined when increasing the engine media supply temperature from 70 to 110 °C, at engine speeds higher than  $n = 1500$  rpm and part load operating conditions. At low engine speeds and high load operations, the friction loss reduction potential is considerably decreased and below 8%, indicating mixed lubrication regimes at the piston group and valve train.

**Keywords:** engine friction; friction measurements; friction loss distribution; subassembly friction; journal-bearing simulation; valve train; journal bearings; piston group

## 1. Introduction

To improve fuel economy and, in particular, the overall mechanical efficiency, the determination of the friction losses of combustion engines is a crucial topic in modern engine development. Based on current challenges for manufacturers including stricter CO<sub>2</sub> emission limits from the legislative side, changing customer preferences (away from product towards function, e.g., car sharing and car rental) and a general focus on the environmental impact, it is nowadays crucial to develop highly efficient vehicles.

Especially for vehicles using internal combustion engines (ICE) which currently deal with bad public reputation due to the Diesel emission scandal, it is very important to present results on how to cut fuel consumption and to limit the exhaust gas emissions. The minimization of the mechanical losses provide a significant contribution to high efficiency vehicles nowadays as well as in the foreseeable future [1]. Measures to reduce the mechanical losses also often show advantages in terms of financial investments compared to hybridization and subsequently increases the overall efficiency of hybrid vehicles [2].

In internal combustion engines, the frictional losses of the base engine are generated by the subassemblies' piston group, crankshaft journal bearings, valve train, timing drive, and shaft seals. This means that friction reduction on these key assemblies continue to represent a significant goal for the development of low-friction base engines. Also, for the first calculations in the concept phase of engine development using empirical friction models [3–5], experimental data for the subassemblies, e.g., of the piston group, under realistic operation conditions is required. Furthermore, the need of advanced lubricant models including the non-Newtonian behaviour and of closer attention to the thermal conditions in the engine when developing engine friction models has been reported in the past [6]. Nowadays, the assessment and assignment of the engine friction losses to the subassemblies is generally done by fired and motored friction tests. Each mentioned measuring method has its area of application with its corresponding advantages and challenges which are briefly described below.

While an engine friction measurement in a fired operation is ideal because of the conventional thermal boundary condition as well as the correct cylinder pressure phasing and gradient, it is challenging to maintain the stability of the engine operation and the repeatability which is required for accurate measurements. Due to the combustion process, one is faced with strongly varying cylinder pressures from cycle to cycle. Furthermore, the inherently high indicated power produces highly alternating torques at the crankshaft. Therefore, a torque transducer with a much larger measurement range is required for a fired operation compared to a motored operation. In References [7,8] an overall methodology is presented which covers a systematic testing procedure from the calibration of the measurement chain to the exact measurement workflows to gain the highest possible repeatability of the conducted tests. Nevertheless, cyclic variations and necessary bigger torque transducer measurement ranges have to be accepted. The developed and used friction measuring module in Reference [8] needs to be specifically designed for the engines put to test. Furthermore, a fired engine operation also has an influence on the used pressure sensors of the cylinder pressure measurement system. Especially, the hysteresis effects during the conducted tests needs to be accounted [8], and the usage of cooled pressure sensors is necessary.

Single-cylinder test beds using the floating-liner principle, on the other hand, are commonly used for direct friction force measurements on the cylinder liner caused by the piston group under fired conditions. One main drawback is the missing possibility to use the conventional crank train of multicylinder engines. The methodology also has to deal with different boundary conditions like limited cylinder pressures, vibrations disturbing the force measurement signals, and stronger cylinder bore distortions due to the design of the test rig. However, in the last years, improvements have been made regarding the sealing system between the floating liner and the cylinder head, and therefore, higher cylinder pressures can be reached. Also, the difference in bore distortions has been minimized in the past using complex measurement and specific honing processes to reach comparable cylinder profiles as in conventional engines [9]. All improvements to enhance the function of the single-cylinder test bed result in high efforts on design and measurement requirements.

The application of conventionally motored (without external charging) engine tests results in a reduced complexity of the test rig due to the missing fuel system. However, very different thermal boundary conditions as well as the absence of a strong cylinder pressure acting on the pistons and bearings are affecting the friction results from these tests. External charging is able to create a mechanical load on the engine that is comparable to a fired operation as well as can be used to create thermal conditions in the

engine that is more similar to a fired operation than it is for conventional motored tests. Although the basic principle of motoring friction tests with external charging is known from the past [10,11], it came up again recently and is currently investigated [12]. Also, developments improving the thermal boundary conditions and reaching comparable load characteristics to a firing operation [13] have been achieved [14,15].

The major advantages of pressurized motoring tests are a significantly higher measurement accuracy due to a strongly reduced indicated mean effective pressure (IMEP; about factor 4 in comparison to a fired operation) and highly stable testing boundary conditions. The cycle-to-cycle cylinder pressure variations in a charged motoring operation are insignificant compared to the fired operation. Therefore, torque transducers with a much smaller measurement range and, consequently, a much higher measurement accuracy can be realized. The external charging is generally realized by supplying pressurized air or inert gases (e.g., nitrogen) to the engine intake. Due to the intrinsic compression of the engine, peak cylinder pressures can be reached which correspond to a conventional fired operation. By using a pressure control valve, the peak cylinder pressure representing the load of the engine can be controlled in a highly variable way which represents an engine operation in part and full load conditions. In contrast to a fired operation, the following limitations are assigned with a pressurized motoring: On the one hand, the position of the maximum cylinder pressure is always very close to the top dead center position of the engine. However, for diesel engines at full load, the resulting position of the pressure maximum occurs about +10 °CA (CA: Crank angle) after TDC (Top dead center) which results in a good agreement between the fired and charged motoring tests when a mechanical load is the dominating factor [15]. On the other hand, the thermal boundary conditions are different for the motoring test due to the missing thermal energy of the combustion processes. This limitation affects the results in particular at part load conditions when comparing the results from friction measurements in fired and pressurized motoring operation [16]. To reduce the lack of thermal energy in the engine during the pressurized motoring test, the charging system can be designed as a recirculation system. Therefore, the engine exhaust is connected to the engine intake. This enables a great increase in the intake temperature of the pressurized air, which subsequently strongly increases the temperature during the compression stroke. This affects the thermal operating conditions especially for the piston group.

For the investigation of further friction reduction measures with the already good friction performance of today's modern engines, methods and tools which can also dissolve and analyze small differences consistently over the operational range of the engines are necessary. To give an example, when analyzing the advantages of (ultra) low viscosity engine oils, deviations in the friction torque of 0.1 Nm have to be resolved over the entire engine operation range [17]. The same can be stated when analyzing small contributors to the friction losses like the crankshaft seals. The highest requirements regarding measurement accuracy and testing workflow have to be met to achieve highly accurate results [18].

Bringing together the advantages of both fields, simulation and testing, can result in new possibilities of analysing engine friction power losses. During the development process of a combined approach at the VIRTUAL VEHICLE Research Center, a friction analysis procedure has been defined which enables very good possibilities for comparisons of measures to reduce engine friction losses [14,15,19]. The developed friction analysis approach combines the results of a detailed elasto-hydrodynamic journal-bearing simulation and charged motoring tests with air recirculation. Due to the combination of simulations and measurements, it is possible to analyse the friction performance of the crankshaft journal bearings, valve train, and piston assembly over the entire engine operation range.

This work presents the application of the developed combined approach using the analysis procedure to investigate the friction losses of a modern passenger-car diesel engine in great detail. The primary aim of the study is to analyse the friction losses of the base engine and its subassembly crankshaft journal bearings, valve train, and piston assembly for different thermal boundary conditions. Therefore, the supply temperatures of oil and cooling water are varied between 70 and 110 °C. These additional investigations,

in particular, at highest temperatures, allow for the potential identification of critical mixed lubrication in subassemblies. The secondary aim is a further breakdown of the friction losses by additional measurements. The individual contribution of the valve train, timing drive, crankshaft seals, and crankshaft main bearings are identified. The measurement of the crankshaft main bearings friction losses enable a verification of the utilization of the journal-bearing simulation approach in a crankshaft system which represents the tertiary aim of this work. The simulation approach was developed on the basis of journal-bearing test-rigs. In this study, the sole measurement of the journal-bearing losses enables a direct comparison with the journal-bearing simulation approach for the first time.

## 2. Friction Losses Analysing Procedure: A Combined Approach Using Experiments and Predictive Journal-Bearing Simulation

The aim of the developed friction loss analysis procedure is the determination of the friction power losses of the base engine for motored and load operations and the breakdown of these losses to the individual components' crankshaft journal bearings, valve train (with timing drive and crankshaft seals), and piston group. For this purpose, an analysis approach combining motored engine test-bed measurements with external charging and a previously developed predictive and widely validated journal-bearing simulation method was developed. An overview of the developed approach is shown in Figure 1.

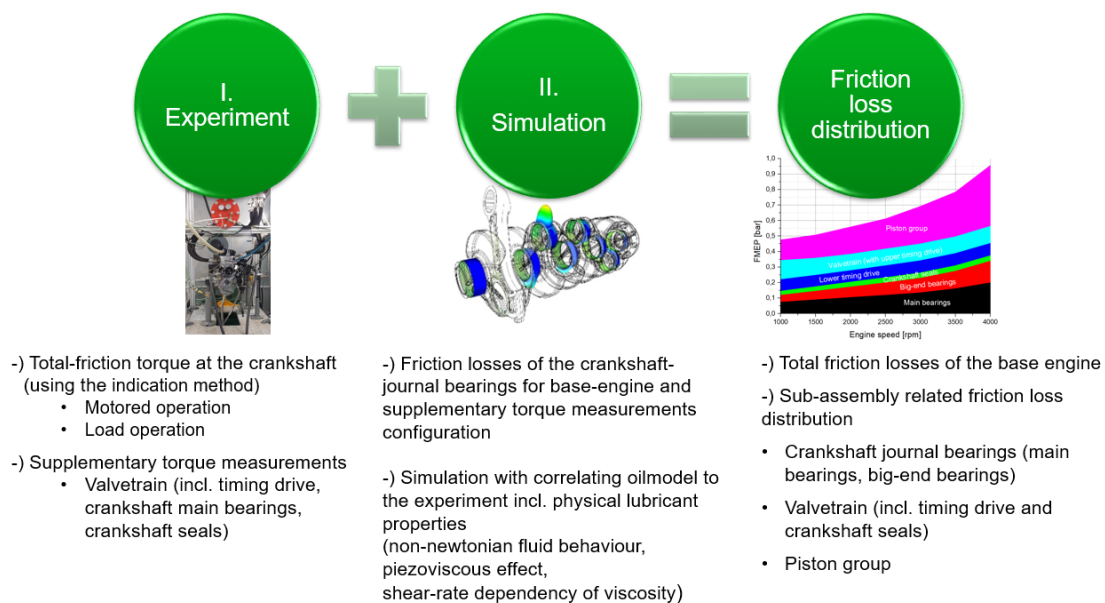


**Figure 1.** A general overview of the used combined approach to analyse the engine friction losses.

The combined approach connects the experimental results with the calculated journal-bearing friction losses from simulation models. This results, on the one hand, in the determination of the base engine total friction losses and, on the other hand, in a subassembly resolved friction loss distribution over the full engine operation range (speed and load).

The measurements are conducted using the indication method (IMEP (Indicated mean effective pressure) method). By using the IMEP-method, the friction losses denoted as FMEP (Friction mean effective pressure) are determined by the subtraction of two similar sized large quantities, the IMEP and the

BMEP (Brake mean effective pressure); see Equation (1). For a motored operation, the signs of IMEP and BMEP are negative in comparison to a fired operation. The FMEP is, in comparison, a rather small quantity.

$$FMEP = IMEP - BMEP \quad (1)$$

Therefore, great care needs to be taken in the determination of the IMEP and BMEP because any significant error in these large quantities can easily lead to a measurement error of the same magnitude as the calculated FMEP. The reduced IMEP (about factor 4 compared to the fired operation) when using charged motoring tests and insignificant cycle-to-cycle variations enable the usage of considerably smaller torque transducers and, therefore, an increased accuracy in BMEP determination. For an accurate IMEP determination, AVL List high-quality industry equipment for cylinder pressure measurements including a 720 ppr rotary encoder system is used. A corresponding calibration of the used measurement equipment is of great importance for reliable and accurate measurements.

*Valve train friction:* In addition to the total base engine friction (FMEP) tests, supplementary friction measurements are done with removed pistons and conrods to obtain the friction torque of the valve train with timing drive and crankshaft seals.

*The simulation of the journal bearing friction losses:* The simulation method is discussed in detail in a later section (Section 4). Here, only the basic applied scheme is outlined. The simulation is prepared in two steps: The first step uses the base-engine simulation model for the calculation of the main bearing and big-end bearing friction losses under the tested operating conditions. In the second step, a reduced engine model without pistons and conrods is used in combination with the supplementary torque measurements of the valve train friction. For detailed and accurate journal-bearing friction loss calculations, it is crucial to use lubricant models which correlate to the experiments and that describe closely the rheological properties of the used engine oil.

To determine the subassembly related friction loss distribution, the following workflow as shown in Figure 2 is used.

The full engine is reduced to the base-engine configuration by removing or deactivating all engine auxiliary devices. This enables to full focus on the base engine friction losses during the friction loss investigations. Before the friction tests are conducted, an extensive running-in procedure is performed to account for the processes affecting the results [20]. The first measurements are then carried out on the base engine to obtain the engine friction map ( $T_{F \text{ Total}}$ ) over the entire load and speed range of interest. The engine friction map is typically measured at different engine media supply temperatures to analyse the influence of different thermal boundary conditions on the friction losses of the engine. Parallel to the experimental part, the journal-bearing simulation model of the base engine is created. Besides the detailed geometrical and mass data of the whole crank train, the interaction between the simulation model and the experiments consists of the cylinder pressure curves and engine speeds for the bearing load and the main bearing temperature measurement data for the journal-bearing simulation methodology. The total friction losses (hydrodynamic and asperity friction losses) of the crankshaft main- and big-end bearings are calculated ( $T_{F \text{ Journal bearings}}$ ) for the same engine operation points as were used in the engine friction map measurements. After the engine friction map measurements are finished, the base-engine is stripped to engine strip-test stage 0 by removing the pistons and conrods. These so-called supplementary torque measurements ( $T_{F \text{ Strip-Test 0}}$ ) are then conducted at the same boundary conditions for the engine speed and engine media supply temperatures as were used for the engine friction map measurements. An additional journal-bearing simulation model in an engine strip-test stage 0 configuration is created to calculate and separate the main bearing friction losses for this strip stage ( $T_{F \text{ Journal bearing Strip-Test 0}}$ ). By subtracting the measured friction torque of the supplementary torque measurements ( $T_{F \text{ Strip-Test 0}}$ ) from the friction torque of the journal-bearing simulation correlating to the supplementary torque measurements ( $T_{F \text{ Journal bearing Strip-Test 0}}$ ), the valve train friction

torque ( $T_{F \text{ Valve train}}$ ) is determined; see Equation (2). Although for simplicity this friction torque is called the valve train friction torque in the following, it is important to note that the (comparatively smaller) friction losses of the timing drive and the crankshaft seal rings are included.

$$T_{F \text{ Valve train}} = T_{F \text{ Strip-Test 0}} - T_{F \text{ Journal bearings Strip-Test 0}} \tag{2}$$

After the determination of the valve train friction losses (Equation (2)), the friction losses of the piston group can be determined. The resulting friction torque of the piston group ( $T_{F \text{ Piston group}}$ ) is calculated from the measured total friction torque of the base engine ( $T_{F \text{ Total}}$ ) by subtraction of the calculated friction torque of the valve train ( $T_{F \text{ Valve train}}$ ) and the calculated friction torque of the crankshaft journal bearings of the base engine configuration ( $T_{F \text{ Journal bearings}}$ ); see Equation (3).

$$T_{F \text{ Piston group}} = T_{F \text{ Total}} - T_{F \text{ Valve train}} - T_{F \text{ Journal bearings}} \tag{3}$$

With this combined approach, it becomes possible to determine the frictional losses of the subassembly piston group, valve train, and crankshaft journal bearings over the full range of engine operation conditions (entire engine speed and load range). This can be done for all kind of single- or multicylinder engines and prototypes, respectively, using conventional reciprocating crank trains. In addition, the cost benefits due to a reduced experimental effort arise, and a detailed insight in the tribological behaviour of the crankshaft main and big-end bearings becomes possible with the journal-bearing simulation results.

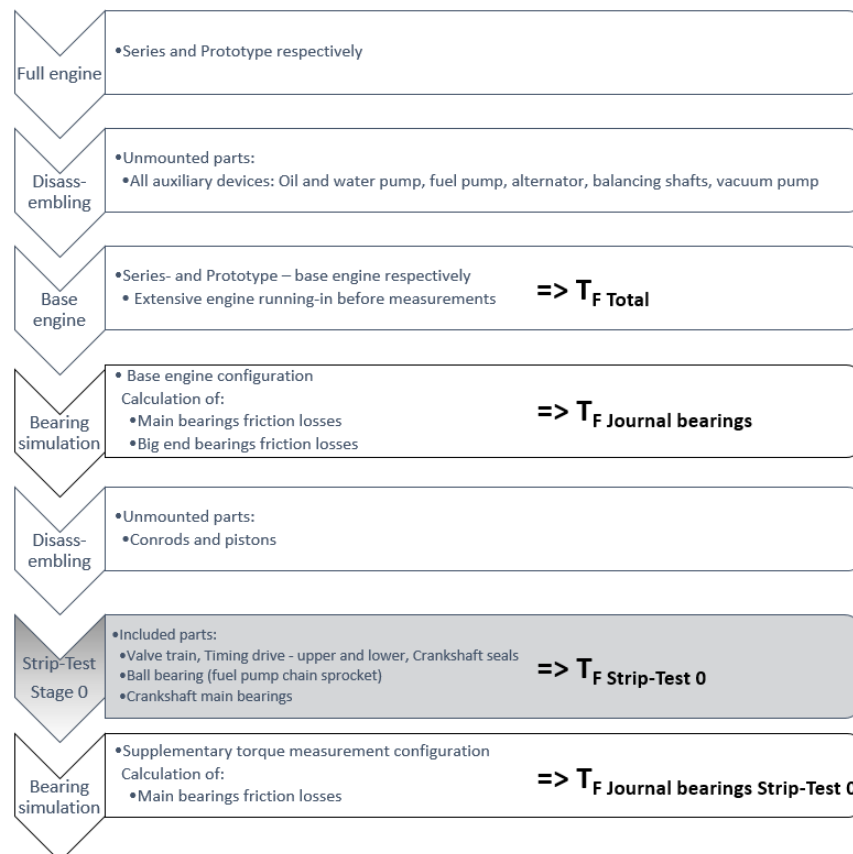


Figure 2. A detailed procedure to determine the subassembly-related friction losses using the combined approach.

### 3. Experimental Investigation

The following subsections give detailed descriptions of the dynamometer, engine preparations, and the testing procedure for the experimental investigations.

#### 3.1. The Dynamometer

The used motored engine test bench with external charging (FRIDA (FRiction DynAmometer)), was developed, designed, and built at the VIRTUAL VEHICLE Research Center. An overview of the experimental setup on the friction dynamometer is given in Figure 3.

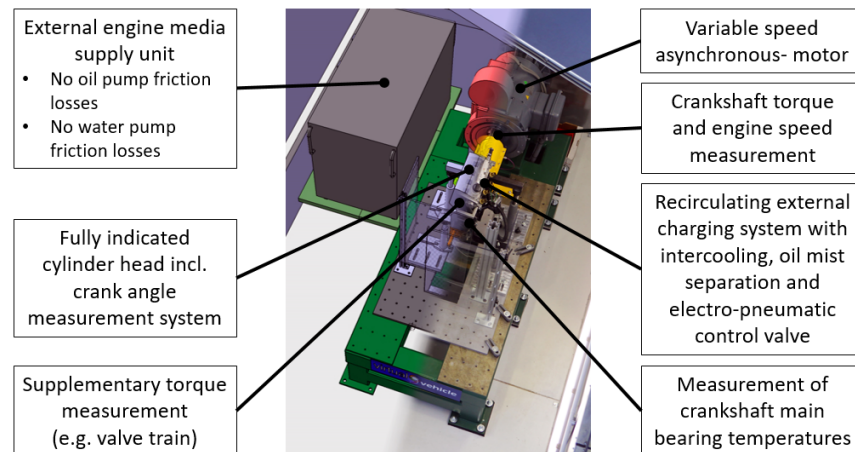


**Figure 3.** An overview of the experimental test setup for the analysis of the engine friction losses.

The fundamental aims of the experimental investigations on the motored engine test bench with external charging are to measure for the determination of the BMEP and the IMEP as well as to allocate the necessary data for the journal-bearing simulation model. For the determination of the BMEP, torque measurements at the crankshaft (brake torque) are conducted. The following equation relates the measured brake torque at the crankshaft ( $T$ ) to the corresponding mean effective pressure ( $BMEP$ ).

$$BMEP = \frac{W}{V_D} = \frac{4\pi T}{V_D}, \quad (4)$$

where  $W$  refers to the work per cycle and  $V_D$  refers to the volume displacement of the investigated 4-stroke engine. A highly accurate torque measurement system with an accuracy class of 0.03 (HBM T12) and integrated speed sensor is used to measure the brake torque and engine speed at the crankshaft. The IMEP determination of the pumping losses according to Equation (5) during the tests is done by integrating the measured cylinder pressure ( $p_{cyl}$ ) over a working cycle divided by the volume displacement of the engine.

$$IMEP = \frac{\int p dV}{V_D}, \quad (5)$$

For the IMEP determination, the cylinder pressures in all four cylinders are measured using piezoelectric pressure sensors (AVL GU12P) which are installed at the glow plug positions by using adapters. The measured piezoelectric charge is processed by a charge amplifier (AVL MicroIFEM). The complete cylinder pressure measurement chain (pressure sensors, cables, and charge amplifier) has been calibrated before the measurements. To allocate the measured cylinder pressure to the particular crank angle an 720 ppr angle encoder (AVL 365C) is used. One crucial point regarding the error sources

in the IMEP determination is the accurate determination of the piston TDC. Even small deviations of the correct TDC position results in large errors in the FMEP determination [21]. Consequently, the TDC determination has to be done with greatest possible precision and, therefore, a capacitive TDC sensor (AVL OT428) was used. The TDC determination using capacitive TDC sensors is one of the most precise techniques which can be used [21]. Ideally, the TDC determination should be done for every single operating point as the engine speed, load, and even the engine media supply temperature influence the exact position of the TDC. Practically, the TDC determination is done for an important engine operating point. For this engine, an engine speed of 2000 rpm and a lubricant supply temperature of 50 °C were selected. The mounted TDC sensor during the TDC determination is shown in Figure 4.

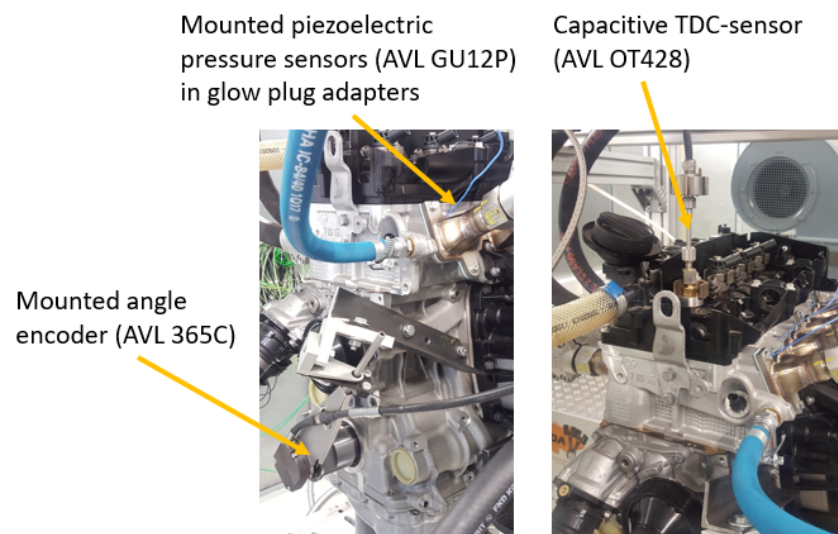


**Figure 4.** The mounted capacitive top dead center (TDC)-sensor and crank angle encoder during the TDC determination.

To obtain the required input data for the journal-bearing simulation and to ensure reproducible testing boundary conditions (thermal and load), an extensive engine preparation and sensor application are necessary which is described in the following subsection.

### 3.2. The Engine under Test and Necessary Engine Preparations

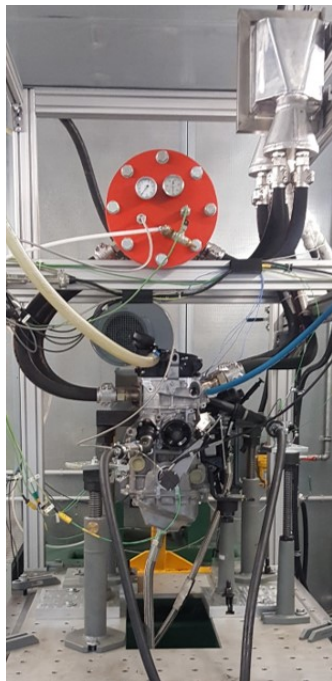
The experimental investigations were carried out for a modern in-line four-cylinder, four-stroke, turbo charged, passenger-car diesel engine with a nominal volume displacement of 2 L and a nominal power of 135 kW. The technical details of the engine are listed in Table 1.

The focus of the conducted friction loss investigation is on the base engine performance and its subassembly piston group, valve train, and crankshaft journal bearings. To analyse the friction losses of the base engine, all auxiliary devices like the oil and water pump, alternator, balancing shafts, vacuum pump, etc. have been removed from the engine or deactivated. Figure 5 shows the engine being installed for the measurements on the dynamometer.

**Table 1.** Technical data of the in-line four-cylinder turbocharged diesel engine under test.

Volume displacement	1995 cm <sup>3</sup>
Compression ratio	16.5:1
Bore	84 mm
Stroke	90 mm
Nominal torque	380 Nm
Nominal Power	135 kW
Maximum Speed	4600 rpm
Cylinder distance	91 mm
Conrod length	138 mm
Main bearing diameter	55 mm
Main bearing width	25 mm
Main bearing mounting clearance	20 μm
Big-End bearing diameter	50 mm
Big-End bearing width	24 mm
Valve-train	DOHC
Timing drive	chain
Valve-train type	roller-type cam follower
Valves	4 per cylinder

It is important to note that all investigations were carried out using a modern SAE (Society of automotive engineers) 5W30 automotive lubricant with an HTHS (High-temperature high-shear-rate viscosity (defined as the dynamic viscosity of the lubricant measured at 150 °C and at a shear rate of 10<sup>6</sup> s<sup>-1</sup>)) viscosity of 3.57 mPas (The detailed oil data are listed in Table 2).

**Figure 5.** The engine on the dynamometer test rig.

The engine oil and coolant are provided by external supply units, and modifications are required on the oil module, oil pan, water pump, and oil- and coolant-circuits. Also, the coolant thermostat has been deactivated to ensure a full coolant flow. Figure 6 shows the deactivated water pump.



**Figure 6.** The deactivated water pump.

The oil and coolant supply temperature and pressures are controlled within  $\pm 0.1$  °C and  $\pm 0.05$  bar, respectively. For the journal-bearing, simulation the main bearing temperatures for all tested operating points are required input parameters besides the measured cylinder pressures and bearing clearances. The bearing temperatures are measured in the high-load zone of the main bearings using type K thermocouples. As shown in Figure 7, three main bearing brackets are equipped with thermocouples.

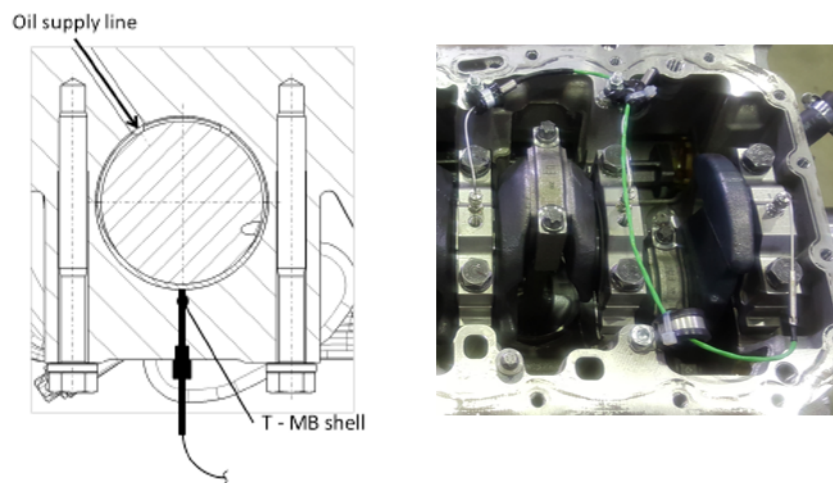


**Figure 7.** The measurement position of the main bearing temperatures: **(left)** A sectional view of the measuring point at the main bearing shell. **(right)** The mounted temperature sensors with cable guiding at the main bearing brackets 1, 2, and 3.

Bearing clearance measurements have been conducted at all five main bearings using measurement gauges. The conducted bearing clearance measurements result in bearing clearances of 20  $\mu\text{m}$ . The high-pressure fuel pump is driven by the crankshaft utilizing a chain sprocket and the lower timing drive. As the friction losses of the fuel pump were not of interest, the connection of the chain sprocket to the pump shaft has been modified. Therefore, a ball bearing was mounted between the fuel pump drive shaft and chain sprocket to deactivate the high-pressure fuel pump drive (see Figure 8).

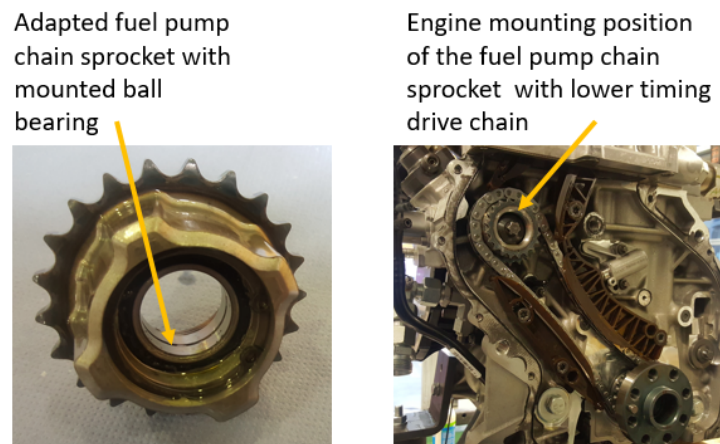


**Figure 8.** The deactivated fuel pump: **(left)** The adapted fuel pump chain sprocket with mounted ball bearing. **(right)** The mounted fuel pump chain sprocket.

During the measurements, only a negligible contribution of the ball bearing comprised the friction torque of the engine [22].

### 3.2.1. Engine Preparations for Additional Torque Measurements

To separate the friction losses of the valve train from the overall base engine friction losses, supplementary measurements were conducted. For this task, the pistons and conrods were removed, and balancing weights were installed on the crank pins (see Figure 9). This was done to compensate the missing rotational mass forces of the conrods and to prevent excessive oil leakage from the otherwise open oil supply bores of the big-end bearings.



**Figure 9.** The mounted balancing weights at the crank pins.

The resulting valve train measurement setup includes the valve train, the timing drive (upper and lower), the ball bearing at the fuel pump chain sprocket, the crankshaft main bearings, and the crankshaft seals. As described in Section 2, the resulting valve train friction losses are calculated using Equation (2).

### 3.2.2. Engine Preparations for Crankshaft Seals Measurements

In the course of the measurement program, the friction torque of the crankshaft radial lip seals were analysed [18]. The measurements were performed with installed and with removed crankshaft seals. For a proper sealing of the engine crankcase during the tests, a simple sealing plug was installed on the FEAD (Front-end auxiliary drive) side of the engine. The sealing plug to seal the engine on the FEAD side is shown in Figure 10.



**Figure 10.** The sealing plug to prevent an oil leakage on the front-end auxiliary drive (FEAD) side of the engine.

A proper sealing of the engine on the flywheel side without a mounted crankshaft seal demands a special sealing apparatus to prevent an oil leakage. For this purpose, a custom sealing case was designed and realized and is shown in Figure 11.

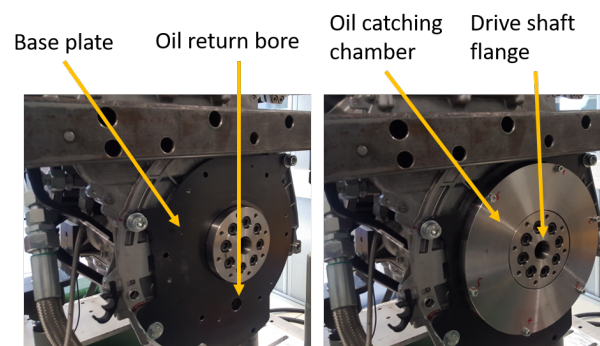


**Figure 11.** The realised crankshaft sealing system on the flywheel side.

For a complete description and detailed information about the realization of the sealing system, refer to Reference [18].

### 3.2.3. Engine Preparations for Crankshaft Measurements

The final strip-stage during the strip-test measurement campaign includes torque measurements of the crankshaft main bearings. Therefore, torque measurements were performed without a timing drive and crankshaft seals. This enables the possibility of comparing the main bearing simulation model with the experimental results of the base engine. For this task, the lower timing drive was deactivated by removing the lower drive chain and by deactivating the chain tension system. Figure 12 shows the engine on the flywheel side with an unmounted timing drive system.



Figure 12. The deactivated timing drive system.

### 3.3. Testing Procedure

To investigate the friction losses of the base engine and its subassembly piston group, valve train, and crankshaft journal bearings, a wide range of tests were conducted. In the first step, engine friction map measurements to determine the FMEP of the base engine over the entire engine operation range were performed, and additional data for the journal-bearing simulation (cylinder pressure curves and journal-bearing temperatures) was collected. After the engine friction map measurements, a four-stage strip-test campaign was performed to determine the frictional losses of the subassemblies and to provide data for a comparison of the journal-bearing simulation results to the measurement results in a motoring operation of the crankshaft.

#### 3.3.1. Measurement Program Base Engine

The base engine measurement program covers 120 different measurement points over a wide range of engine speeds and load points for three different engine media supply temperatures of 70 °C, 90 °C, and 110 °C. This results in detailed engine friction maps for different engine media supply temperatures. Figure 13 shows the performed measurement program both in the motored and load conditions.

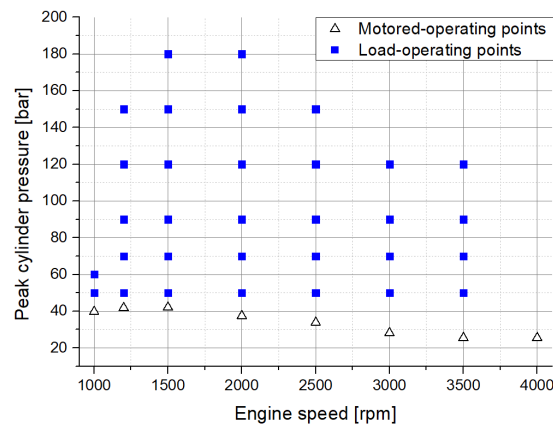
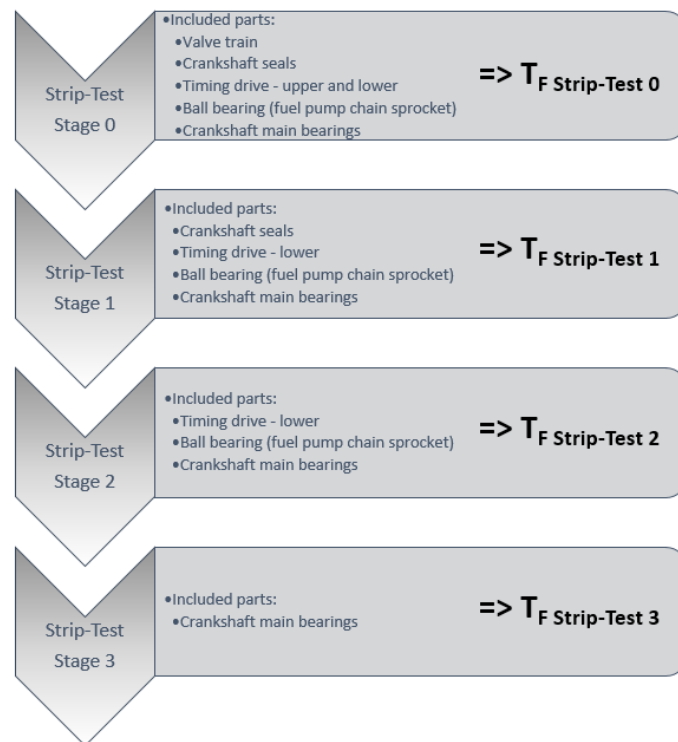


Figure 13. The realized measurement program (motored- and load-operating points).

### 3.3.2. Additional Measurements: Strip-Test Procedure

To determine the frictional losses of the subassemblies, typically just one strip-test stage (strip-test stage 0) is necessary when applying the combined approach. Nevertheless, for this engine, additional measurements have been conducted to further separate the friction losses of the crankshaft seals, lower timing drive, and crankshaft journal bearings experimentally. Therefore, an extended strip-measurement campaign covering three additional strip-test stages has been conducted (see Figure 14). All strip-test stages have been investigated experimentally at engine media supply temperatures of 70 °C, 90 °C, and 110 °C to give detailed insight into the friction behaviour of the assemblies and components working under different thermal boundary conditions.



**Figure 14.** The measurement campaign for the additional torque measurements to determine the frictional losses of the subassemblies.

In the first strip-test stage (strip-test stage 0), the tests are performed after dismounting all pistons and conrods as well as all auxiliary devices (see Figure 2) resulting in friction torque  $T_{F \text{ Strip-Test } 0}$  which represents the basis for the determination of the valve train friction losses using the combined approach (see Equation (2)). In the next strip-test, stage 1 torque measurements are conducted without the valve train and the upper timing drive resulting in friction torque  $T_{F \text{ Strip-Test } 1}$ . Equation (6) is used to calculate the resulting friction torque of the valve train and upper timing drive.

$$T_{F \text{ Valve train and upper timing drive}} = T_{F \text{ Strip-Test } 0} - T_{F \text{ Strip-Test } 1} \tag{6}$$

After strip-test stage 1, the crankshaft radial lip seals have been dismantled and the friction torque  $T_{F \text{ Strip-Test } 2}$  was measured in strip test stage 2. The friction torque of the crankshaft seals are the results of using Equation (7) by a subtraction of the measured torques of strip-test stage 1 and strip-test stage 2.

$$T_{F \text{ Crankshaft seals}} = T_{F \text{ Strip-Test } 1} - T_{F \text{ Strip-Test } 2} \tag{7}$$

Finally, in strip-test stage 3, the lower timing drive was unmounted and the friction torque  $T_{F \text{ Strip-Test } 3}$  of the crankshaft main bearings solely was measured. The friction losses of the lower timing drive are calculated using Equation (8).

$$T_{F \text{ Lower timing drive}} = T_{F \text{ Strip-Test } 2} - T_{F \text{ Strip-Test } 3} \tag{8}$$

The particular results of the strip-measurements are plotted and discussed in the measurement results section.

### 3.4. Measurement Results

In this section, the results of the experimental investigations on the passenger-car diesel engine are presented. The measurement results are organised in the results of the base engine (engine friction maps) and the results of the conducted strip-measurement campaign. Due to the different engine media supply temperatures of 70 °C, 90 °C, and 110 °C, the influence of increased lubricant temperatures resulting in a lower lubricant viscosity is analysed.

#### 3.4.1. Results Base Engine

The base engine friction map results are obtained at three different engine media supply temperatures covering 120 different measurement points. The resulting engine friction maps of the base engine are shown in Figure 15.

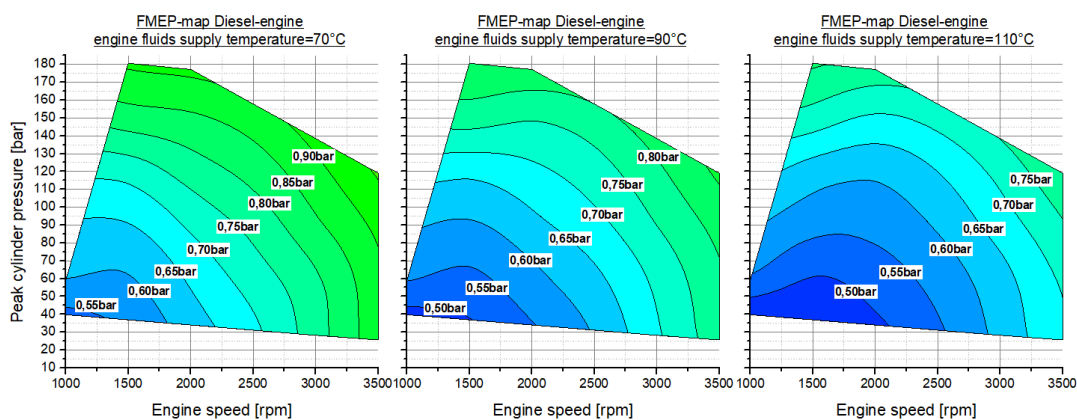


**Figure 15.** The resulting friction mean effective pressure (FMEP) maps for different engine media supply temperatures: **(left)** Supply temperature = 70 °C. **(middle)** Supply temperature = 90 °C. **(right)** Supply temperature = 110 °C.

The FMEP level of the modern diesel engine is generally low and comprises a good base engine performance regarding the mechanical efficiency. It is interesting to note that the highest FMEP-levels result at the lowest lubricant supply temperature of 70 °C and the lowest are at the highest lubricant supply temperature of 110 °C. The highest FMEP value of FMEP = 0.96 bar has been identified at an engine

speed of  $n = 3500$  rpm and a peak cylinder pressure of 120 bar at an engine media supply temperature of  $70\text{ }^{\circ}\text{C}$ . The lowest FMEP results at the lowest engine speed of  $n = 1000$  rpm with  $\text{FMEP} = 0.46$  bar at the motored engine operation ( $p_{\text{cyl}} = 40$  bar) at an engine media supply temperature of  $110\text{ }^{\circ}\text{C}$ . With an increasing engine media supply temperature, the FMEP-level decreases over the entire engine speed and load range. By subtraction of the individual FMEP results between the different engine media supply temperatures, the friction reduction potential when increasing the engine media supply temperature can be calculated (see Figure 16).

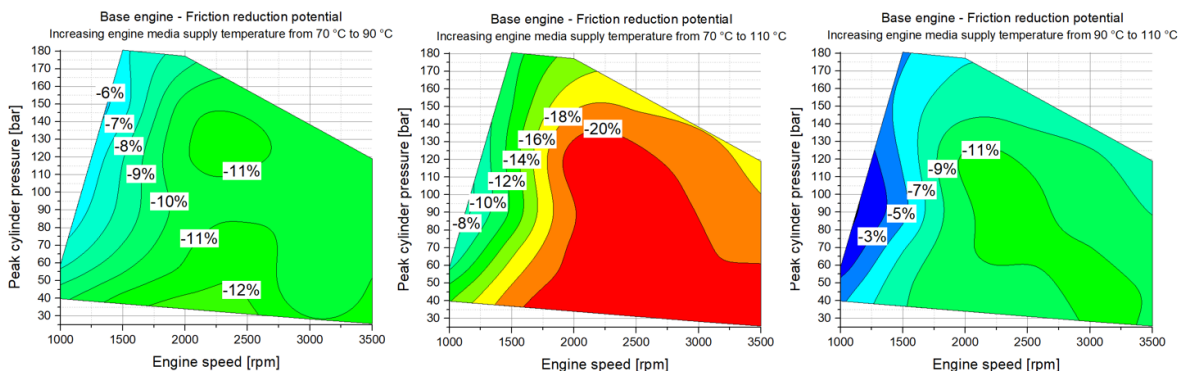


**Figure 16.** The friction reduction potential at the base engine when increasing the engine media supply temperature.

The increase in the engine media supply temperature shows advantages in the FMEP over the entire engine speed and load range. When increasing the engine media supply temperature from  $70\text{ }^{\circ}\text{C}$  to  $90\text{ }^{\circ}\text{C}$ , advantages up to 13% are investigated. At low engine speeds, the advantages of the FMEP are in the range of 6%. When increasing the engine media supply temperature from  $70\text{ }^{\circ}\text{C}$  to  $110\text{ }^{\circ}\text{C}$ , advantages of up to 21% in FMEP over a large area ranging from an engine speed of  $n = 1500$  rpm up to  $n = 3500$  rpm at part load conditions are observed. While the advantages at engine speeds higher than  $n = 1500$  rpm are above 16%, they decrease at lower engine speeds. At an engine speed of  $n = 1000$  rpm and load operation, the advantage in FMEP is 8%. It was further found that, when increasing the engine media supply temperature from  $90\text{ }^{\circ}\text{C}$  to  $110\text{ }^{\circ}\text{C}$ , the advantage at an engine speed of  $n = 1000$  rpm is below 2% at load conditions.

The required journal-bearing temperatures for the journal-bearing simulations are measured in main bearings 1, 2, and 3 during all conducted measurements. Figure 17 shows the resulting temperatures at the main bearing shells in the high loaded zone (see Figure 7) determined during the engine friction map measurement campaign at an lubricant supply temperature of  $90\text{ }^{\circ}\text{C}$ .

As expected, the bearing temperatures show an influence on the engine speed and engine load whereupon the influence on the engine load is less distinctive. The highest bearing temperature was determined at an engine speed of  $n = 3500$  rpm and high load conditions with  $107\text{ }^{\circ}\text{C}$  at main bearing 1. It is also interesting to note that the influence on the engine speed is less distinctive at main bearing 2. While at an engine speed of  $n = 3500$  rpm, the main bearing temperature, at main bearing 1 and main bearing 3 are identical with  $105.4\text{ }^{\circ}\text{C}$ ; the temperature at main bearing 2 is  $100\text{ }^{\circ}\text{C}$ . The results show that bearing temperature measurements at just one main bearing can lead to differences up to  $5\text{ }^{\circ}\text{C}$  in bearing temperature which are provided as input data to the journal-bearing, simulation affecting the calculated results of the journal-bearing friction losses.

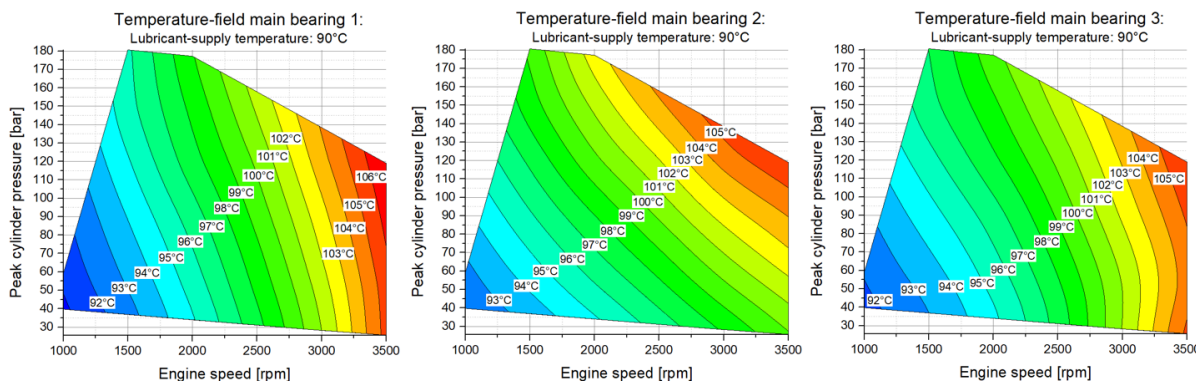


Figure 17. Measured main bearing temperatures: (left) Main bearing 1. (middle) Main bearing 2. (right) Main bearing 3.

### 3.4.2. Results Strip-Tests

The results of the strip-measurement campaign are presented under motored conditions ranging from an engine speed of  $n = 1000$  rpm to  $n = 4000$  rpm for three different engine media supply temperatures:  $70\text{ }^{\circ}\text{C}$ ,  $90\text{ }^{\circ}\text{C}$ , and  $110\text{ }^{\circ}\text{C}$ . The results presented are the the calculated results of the individual strip-test stages from Equations (6)–(8) for the friction losses of the valve train (including the upper timing drive), crankshaft seals, and lower timing drive respectively. The individual measurement results of the strip-test stages are presented in Appendix A (Figures A1–A4).

Figure 18 shows the resulting friction torque of the valve train (including the upper timing drive) for three different engine media supply temperatures.

For engine speeds higher than  $n = 1500$  rpm, the friction losses of the valve train and upper timing drive are almost constant over an engine speed ranging between  $1.6\text{ Nm}$  and  $1.75\text{ Nm}$ . At engine speeds lower than  $n = 1500$  rpm, the friction torque shows a dependence on the engine media supply temperature. With an increasing engine media supply temperature, the friction torque also increases. Compared to  $1.8\text{ Nm}$  at a supply temperature of  $70\text{ }^{\circ}\text{C}$ , the friction torque increases for a supply temperature of  $90\text{ }^{\circ}\text{C}$  and  $110\text{ }^{\circ}\text{C}$  to  $2\text{ Nm}$  and  $2.1\text{ Nm}$ , respectively. This indicates beginning mixed lubrication regimes at the investigated subassembly valve train (including the upper timing drive).

The outcome of the investigation of the crankshaft seals friction losses are presented in another publication and for further informations, refer to Reference [18]. For the sake of completeness, the resulting friction torque of the crankshaft seals are shown in Figure 19 for different engine media supply temperatures.

The determined friction losses of the lower timing drive are plotted in Figure 20 for  $70\text{ }^{\circ}\text{C}$ ,  $90\text{ }^{\circ}\text{C}$ , and  $110\text{ }^{\circ}\text{C}$  engine media supply temperatures.

The friction torque of the lower timing drive is almost constant over the engine speed range from  $n = 1000$  rpm to  $n = 4000$  rpm ranging from  $1.1\text{ Nm}$  to  $1.3\text{ Nm}$ . A slight supply temperature dependence of the friction torque at engine speeds below  $n = 2000$  rpm with differences in the friction torque of  $0.14\text{ Nm}$  between supply temperatures of  $70\text{ }^{\circ}\text{C}$  and  $110\text{ }^{\circ}\text{C}$  was investigated. With an increasing engine media supply temperature, the friction torque increases from  $1.1\text{ Nm}$  at  $n = 1000$  rpm and a supply temperature of  $70\text{ }^{\circ}\text{C}$  to  $1.24\text{ Nm}$  at a supply temperature of  $110\text{ }^{\circ}\text{C}$ . The friction torque results for a supply temperature of  $90\text{ }^{\circ}\text{C}$  are located between the results of  $70\text{ }^{\circ}\text{C}$  and  $110\text{ }^{\circ}\text{C}$  with  $1.18\text{ Nm}$ . The friction torque of the lower timing drive also includes the friction loss of the ball bearing of the fuel pump chain sprocket. The grease-lubricated grooved ball bearing friction losses can be predicted from the manufacturers’ information and literature. It is a minor friction contributor with a range of friction torque between  $0.02\text{ Nm}$  to  $0.04\text{ Nm}$  depending on the engine speed [22].

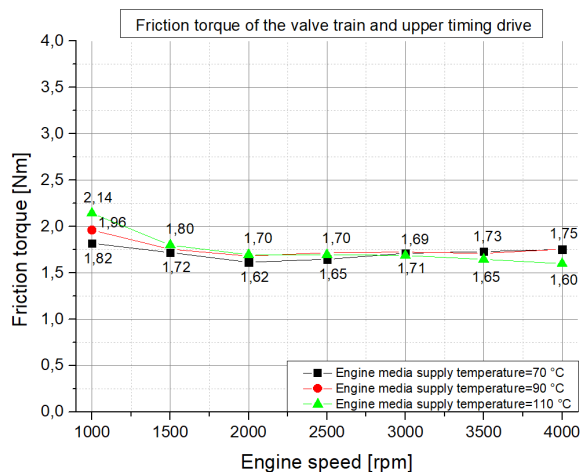


Figure 18. The resulting friction torque for different engine media supply temperatures: The valve train and upper timing drive using Equation (6).

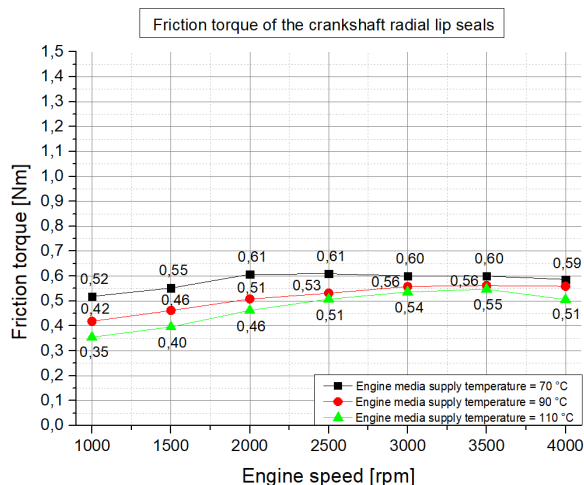


Figure 19. The resulting friction torque for different engine media supply temperatures: The crankshaft seals.

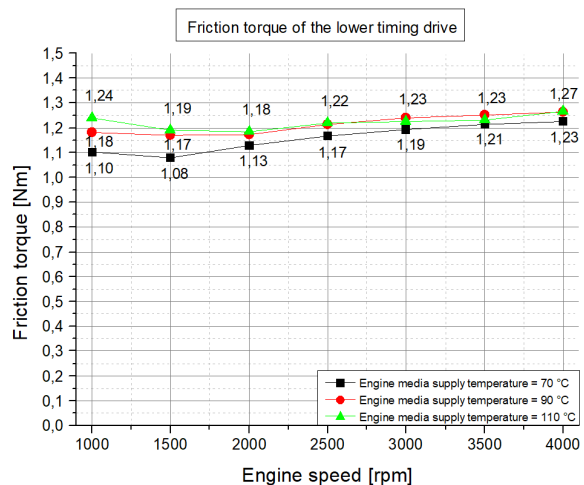
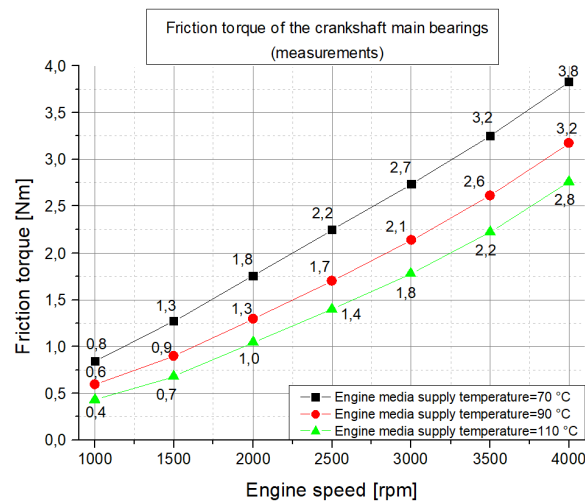


Figure 20. The resulting friction torque for different engine media supply temperatures: The lower timing drive.

The last step of the strip-test campaign enables the investigation of the friction losses of the crankshaft main bearings in a strip-test configuration. Due to the used sealing system for measurements without mounted crankshaft seals, the friction torque of the main bearings solely can be obtained. Figure 21 shows the friction torque of the crankshaft main bearings over the engine speed for different engine media supply temperatures.



**Figure 21.** The resulting friction torque for different engine media supply temperatures: The crankshaft main bearings.

As expected, a strong influence of the engine speed was derived from the friction torque results plotted in Figure 21. Furthermore, a decrease in the friction torque with an increasing engine media supply temperature was investigated. The lowest friction torque occurs at the highest supply temperature of 110 °C ranging from 0.4 Nm at an engine speed of  $n = 1000$  rpm to 2.8 Nm at an engine speed of 4000 rpm. The highest friction torque occurs at the lowest lubricant supply temperature of 70 °C ranging from 0.8 Nm at 1000 rpm to 3.8 Nm at 4000 rpm. The obtained friction torque measurements of the crankshaft main bearings can also be used for a verification of the calculated journal-bearing friction losses from the used simulation methodology. The results of the verification are presented in Section 4.1.

#### 4. Journal-Bearing Friction Loss Simulation

The simulation approach for determining the friction losses of the crankshaft journal bearings consists basically of an elastic multi-body simulation with an isothermal description of the oil film using the Reynolds equation in combination with the approach of Greenwood and Tripp to describe the metal-to-metal contact. The simulation methodology was realised in numerous long-term research projects. It is capable of calculating the friction losses in journal bearings accurately as could be shown in a direct comparison to the experimental data [23,24]. In previous works, a wide range of aspects have been investigated and discussed like the extension of the simulation model to TEHD (Thermo elasto hydro dynamic) [25] simulations under severe mixed lubrication [26] or journal bearing simulations with new engine operation technologies like start/stop systems [27]. Also, the investigation of friction reduction potentials using low viscosity lubricants as well as the resulting possible risks due to increased mixed lubrication regimes have been conducted in the past using the developed simulation methodology [28,29]. In the following, a short summary is reproduced here for brevity, and for a rather complete overview, we refer to References [30–32]. To calculate the journal-bearing friction losses of the engine using the developed simulation approach, an engine model based on the MBS (Multi-body system) AVL Excite Power Unit (AVL EXCITE Power

Unit Version 2017.1, AVL List GmbH, Advanced Simulation Technology, Hans-List-Platz 1, 8020 Graz, Austria, [www.avl.com](http://www.avl.com).) was set up for the engine. The engine model consists of condensed FE (Finite element) structures of the crankshaft, main bearings, and connecting rods, with all bodies being elastically deformable and mass carried [33,34]. The following Figure 22 shows the schematic structure of the engine model for the journal-bearing simulations.

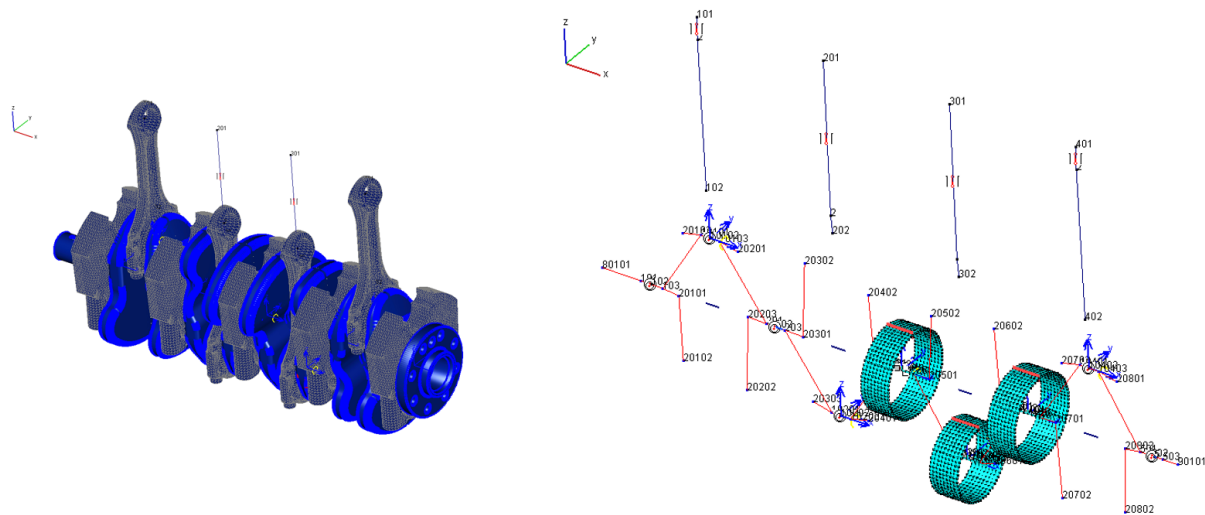


**Figure 22.** The engine model for the journal-bearing simulation: (left) The Finite Element model. (right) The condensed model.

Besides the geometrical dimensions (macro- and micro-geometry), the required input data for the journal-bearing simulation model are the main and big-end bearing temperature, the lubricant supply temperature and pressure, the cylinder pressure profile over the crank angle, and the engine speed which are provided from the experimental investigations on the motored test rig. The basic physical properties of the SAE 5W30 lubricant used in this work are listed in Table 2.

**Table 2.** The basic rheological properties of the lubricant.

SAE class	5W30
Density at 15 °C	853 kg/m <sup>3</sup>
Dynamic viscosity at 40 °C	59.88 mPas
Dynamic viscosity at 100 °C	9.98 mPas
HTHS viscosity	3.57 mPas

HTHS: high-temperature high-shear-rate viscosity (defined as the dynamic viscosity of the lubricant measured at 150 °C and at a shear rate of 10<sup>6</sup> s<sup>-1</sup>).

To describe the physical properties of the lubricant in the simulation model, an extensive rheological model is employed [35]. For the description of the pressure- and temperature-dependent density, the widely used Dowson/Higginson equation is used (see Equation (9)), applying the parameters listed in Table 3.

$$\rho(p, T) = \rho_0 \cdot \left( 1 + \frac{f_1 \cdot p}{1 + f_2 \cdot p} \right) \cdot (1 - f_3 \cdot (T - T_0)) \tag{9}$$

Finally, Figure 23 shows the calculated density vs. temperature relation of the lubricant for different contact pressures.

**Table 3.** The rheological parameters for Equation (9) of the SAE 5W30 lubricant.

$\rho_0$	853	kg/m <sup>3</sup>
$T_0$	15	°C
$f_1$	0.001	1/MPa
$f_2$	0.003	1/MPa
$f_3$	$8.5 \times 10^{-4}$	1/°C

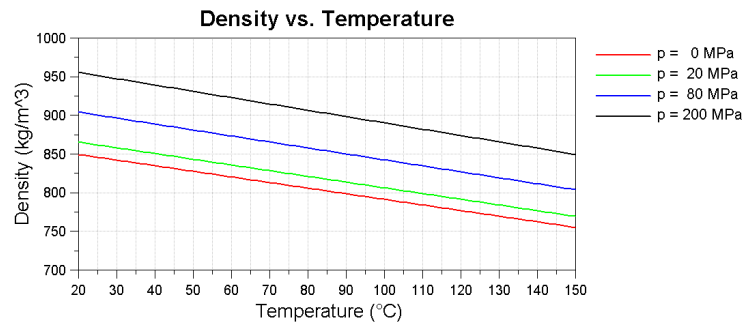


**Figure 23.** The calculated lubricant density.

Besides the description of the density–pressure relation using Equation 9, the description of the physical properties describing the influence on lubricant viscosity, the temperature dependence, the pressure dependence (piezoviscos effect), and the non-Newtonian behavior (the dependence of the viscosity on the local shear rate) of the modern multigrade lubricant is comprehensively taken into account in the calculation [24,36]. Using the Vogel equation [37] for the dependence on the temperature ( $T$ ), the Barus equation [38] for the piezoviscous behaviour ( $p$ ), and the Cross equation [39] to describe the influence of the shear-rate ( $\dot{\gamma}$ ), the influences on the viscosity ( $\eta$ ) can be described using Equation (10).

$$\eta(T, p, \dot{\gamma}) = A \cdot e^{\frac{B}{T+C}} \cdot e^{\alpha \cdot p} \cdot \left( r + \frac{1 - r}{1 + (K \cdot \dot{\gamma})^m} \right) \tag{10}$$

The applied parameters are listed in Table 4 and are calculated using results from previously published work [24] and from lubricant characteristics obtained from a conducted laboratory oil analysis.

**Table 4.** The rheological parameters for Equation (10) of the SAE 5W30 lubricant.

A	0.064	mPas
B	1124.7	°C
C	125.48	°C
m	0.79	-
$\alpha$	0.0009	1/bar
r	0.75	-
K	$3.5 \times 10^{-7}$	s

The computed viscosity behaviour including the influences of the lubricant temperature, contact pressure, and shear-rates are plotted in Figure 24.

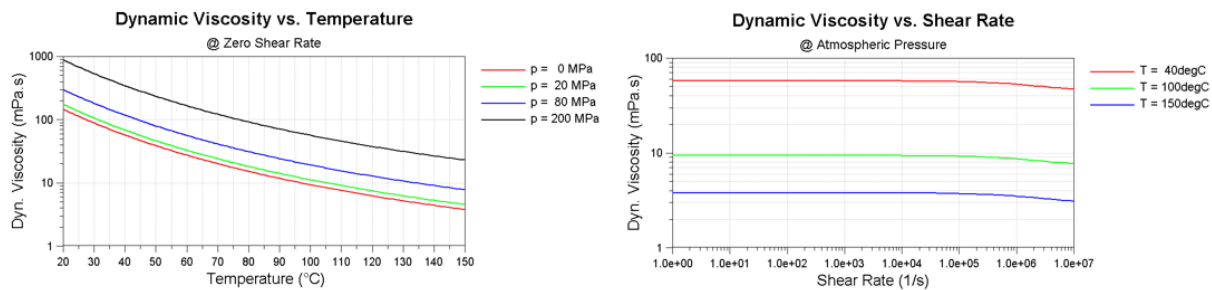


**Figure 24.** Lubricant viscosity dependences: (left) The viscosity–temperature curve for different contact pressures. (right) The viscosity–shear rate curves for different temperatures.

As the simulation model is carried out as an EHD (Elasto hydro dynamic)-calculation, a global bearing temperature has to be defined, which represents a suitable compromise for the entire journal bearing (hot oil temperature in the high loaded zone and cooler oil temperature in the non-loaded zone). In recent projects, a methodology to calculate an equivalent temperature was developed [24,25]. Therefore, thermal processes and heat flows have been investigated [25] using measurements and simulations. To describe the equivalent temperature of the journal bearing, measured temperatures (oil supply temperature and main bearing shell temperature) are used.

$$T_{\text{Equiv}} = T_{\text{MB Shell}} - \left( \frac{T_{\text{MB Shell}} - T_{\text{MB Supply}}}{4} \right) \quad (11)$$

where  $T_{\text{MB Supply}}$  is the lubricant supply temperature and  $T_{\text{MB Shell}}$  is the temperature in the high load zone of the main bearing. Using Equation (11) results in the equivalent temperature of the journal bearing.  $T_{\text{MB Supply}}$  and  $T_{\text{MB Shell}}$  are provided from the experimental investigations on the motored test rig. By applying temperature sensors at the individual main bearings during the experiments (see Figure 7), the equivalent main bearing temperatures of the individual main bearings can be calculated and provided to the journal-bearing simulation model. Due to the higher loads acting on the big-end bearings, they have to work at increased temperatures compared to the main bearings. Published experimental data show an increase in the big-end temperature at the bearing shell of about 3–5 °C compared to the main bearings [40]. Nowadays, modern diesel engines work under much higher bearing loads, and therefore, a further increase of the big-end bearing temperatures is expected. Recent results from measurements at journal-bearing test rigs confirm these expectations [23,24]. For that reason, the temperatures of the big-end bearings are approximated to be about 7 °C higher than the calculated equivalent temperatures of the main bearings. Figure 25 shows the resulting equivalent bearing temperature for main bearing 2 and the big-end bearing 2. For the sake of completeness, the calculated equivalent bearing temperatures for main bearing 1 and main bearing 3 are presented in Appendix A in Figure A5.

While the adjustment of a few single degree Celsius only has a marginal influence on the results, the usage of the measured main bearing shell temperatures is significant because the deviation between the oil supply temperature and bearing shell temperature can easily be above 20 °C, resulting in major reductions of the lubricant viscosity (see Figure 24). As can be seen from the shown temperatures, there is a strong dependence on the engine speed and load present that counteracts the increase in the friction power losses of the journal bearings at high engine speeds and loads.

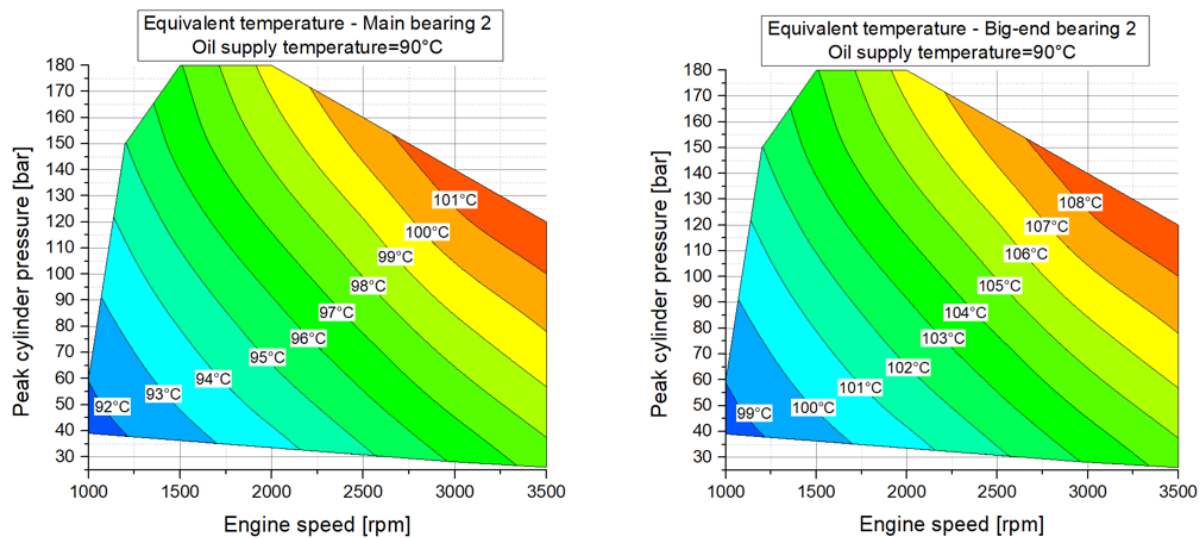


**Figure 25.** The equivalent temperatures for the isothermal journal-bearing simulation for main bearing 2 and big-end bearing 2 calculated using Equation (11).

4.1. Simulation Results

The calculation of the journal-bearing friction losses using the developed simulation methodology was carried out for the equal engine operation points of the measurement campaign (see Figure 13) for three different engine media supply temperatures: 70 °C, 90 °C, and 110 °C. Consequently, 120 different engine operation points have been calculated to obtain the crankshaft journal-bearing friction losses. The resulting FMEP of the main- and big-end bearings for an engine media supply temperature of 90 °C is shown in Figure 26.

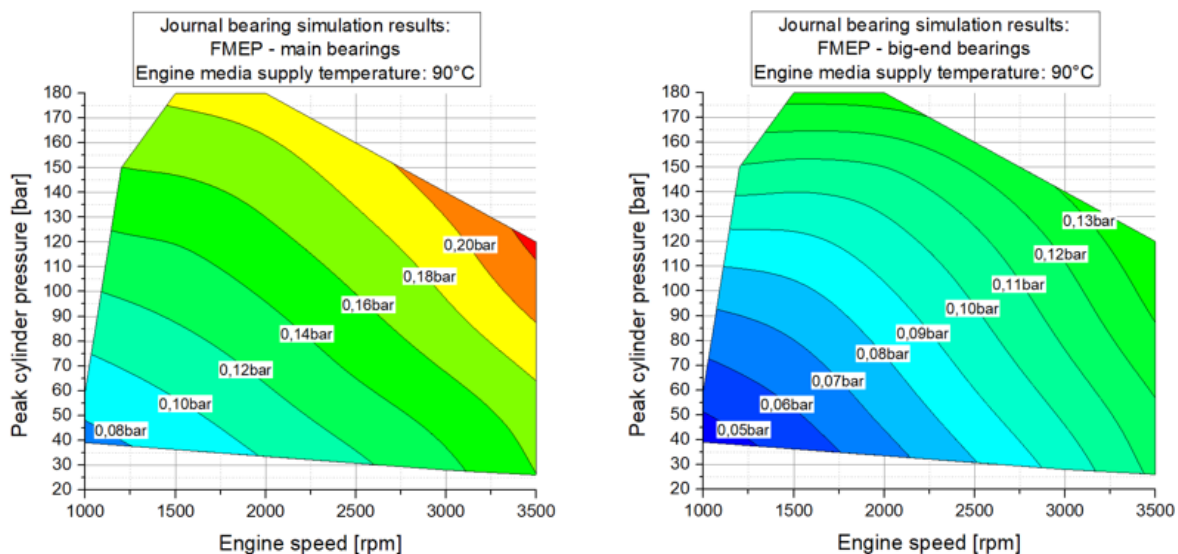


**Figure 26.** The resulting FMEP using the journal-bearing simulation method: (left) Main bearings. (right) Big-end bearings.

The results in Figure 26 show the determined FMEP of the five main bearings ranging from 0.07 bar at an engine speed of  $n = 1000$  rpm in a motored operation to 0.23 bar at an engine speed of  $n = 3500$  rpm

at an peak cylinder pressure of 120 bar. The friction losses of the four big-end bearings range from 0.04 bar at an engine speed of  $n = 1000$  rpm in a motored operation to 0.14 bar at an engine speed of  $n = 3500$  rpm at a peak cylinder pressure of 120 bar. The resulting FMEP of the main and big-end bearings at a lubricant supply temperature of  $70\text{ }^{\circ}\text{C}$  and  $110\text{ }^{\circ}\text{C}$  can be found in Appendix A for the sake of completeness and are plotted in Figures A6 and A7. In addition, it is interesting to investigate the friction reduction potential when increasing the engine media supply temperature. Due to the calculation at different lubricant supply temperature levels,  $70\text{ }^{\circ}\text{C}$ ,  $90\text{ }^{\circ}\text{C}$ , and  $110\text{ }^{\circ}\text{C}$ , this was realized and the results are shown in Figure 27.

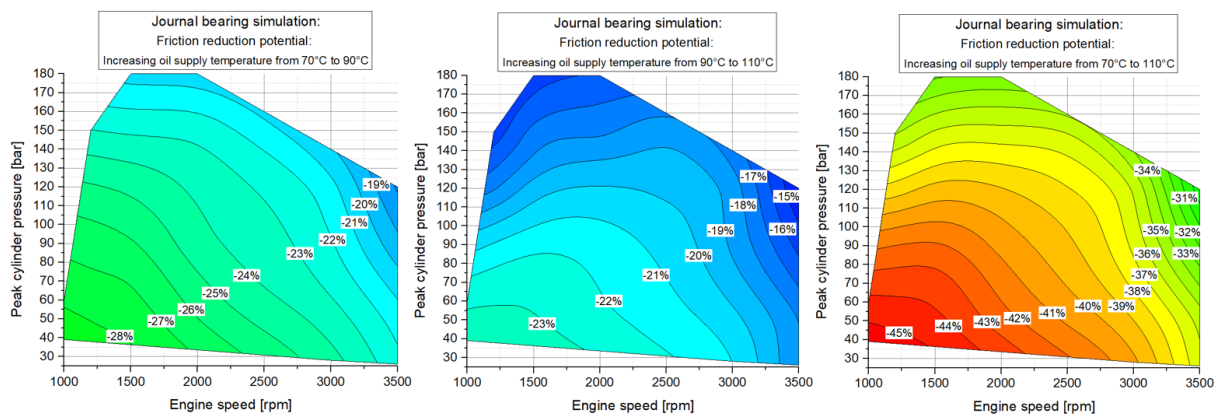


**Figure 27.** The friction reduction potential when increasing the oil supply temperature.

The most significant friction reduction potential for the crankshaft journal bearings has been observed when the supply temperature is increased from  $70\text{ }^{\circ}\text{C}$  to  $110\text{ }^{\circ}\text{C}$  at engine speeds below  $n = 2000$  rpm and at peak cylinder pressures smaller 80 bar. Here, the maximum friction reduction with more than 45% could be determined. It was further found that, at the crankshaft journal bearings, no mentionable mixed lubrication regime occurred over the entire investigated engine speed and load range.

#### Simulation Results: Supplementary Torque Measurement Configuration (Strip-Test Stage 0)

To obtain the valve train friction losses using Equation (2) of the developed combined friction breakdown approach, the journal-bearing friction losses at the engine configuration for strip-test stage 0 (without pistons and conrods but with the mass of the master weights at the crank pins) have been calculated. The resulting FMEP of the journal-bearing simulations in a strip-test stage 0 configuration is shown in Figure 28 over the engine speed for different lubricant supply temperatures.

When comparing the calculated journal bearing friction losses to the results from the conventional base engine model, the strip-test stage 0 configuration shows a decreased FMEP level. This can be stated to the missing load transmitted by the pistons and conrods, which are not installed during the strip-test stage 0 investigations. Also, a clear temperature dependency is found in Figure 28, where the highest friction losses occur at the lowest lubricant supply temperature and the lowest friction levels are investigated at the highest supply temperature. A possible explanation for this result is the decreasing viscosity of the lubricant with an increasing temperature (see Figure 24), which yields a strong decrease of the hydrodynamic friction losses. In addition, high shear rates at high engine speeds are further responsible for a decreasing behaviour of the lubricant viscosity, which results in a continuing reduction of the journal-bearing friction losses as long as no severe mixed lubrication is present.

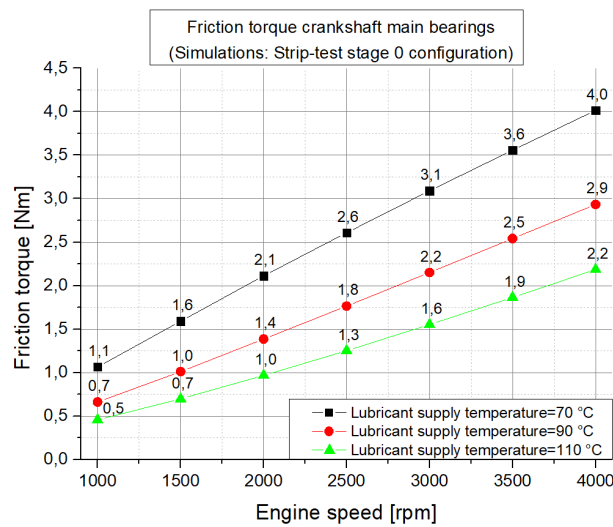


**Figure 28.** The resulting friction torque using the journal-bearing simulation method: The strip-test stage 0 configuration.

Another investigation using the calculated friction losses of the journal-bearing simulation can be conducted when performing comparisons to the conducted measurements. Therefore, the results of the calculations with the journal-bearing simulation model in the strip test stage 0 configuration (see Figure 28) have been compared to the measurement results in the engine strip-test stage 3 configuration (see Figure 21). Figure 29 shows the comparison carried out for a lubricant supply temperature of 90 °C.

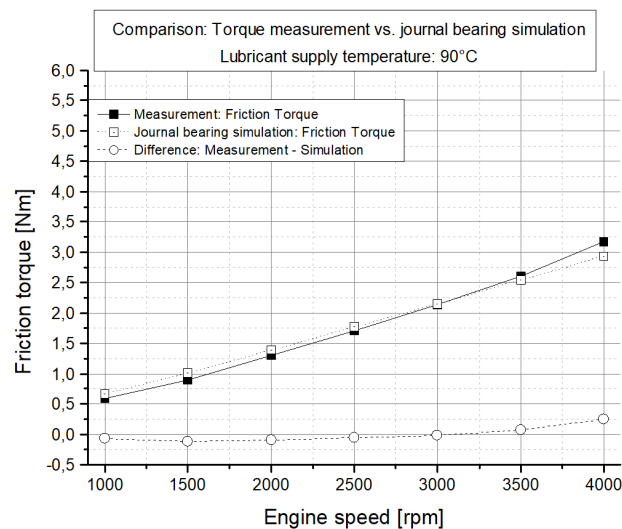


**Figure 29.** A comparison between the measurement and journal-bearing simulation for a lubricant supply temperature of 90 °C.

The comparison of the journal bearing simulation with the measurement data shows a good compliance over the investigated engine operation points. The deviation in friction torque between the measurement and simulation at an lubricant supply temperature of 90 °C is within 0.1 Nm up to an engine speed of  $n = 3500$  rpm and 0.24 Nm at  $n = 4000$  rpm. It is important to mention that no specific matching between the developed simulation methodology and the measurement results has

been conducted. For brevity, the comparison for a lubricant supply temperature of 70 °C and 110 °C are presented in Appendix A in Figure A8.

Summarizing, it is concluded that the conducted comparisons between the measurements in strip-test stage 3 and the journal-bearing simulation represent the worst case scenarios for the developed journal-bearing simulation methodology. The reason for that is that the validation process during the development of the journal-bearing simulation model has been performed with the experimental data from journal-bearing test-rig measurements where the bearing load is a dominant factor for the resulting journal-bearing friction losses. For that reason, it can be expected that the calculation results of the journal-bearing friction losses are significantly improved for load conditions using the simulation model of the base engine including the conventional crank train.

### 5. Applying the Combined Approach: A Subassembly-Resolved Friction Loss Distribution

In the following section, the results of the friction loss investigations conducted in the passenger-car diesel engine (for specifications, see Table 1) using the combined approach are presented and discussed. In the first part, the results of the valve train friction losses (including the timing drive and crankshaft seals) using the combined friction analysis approach will be presented. In the second part, the subassembly-resolved friction analysis of the base engine, namely crankshaft journal bearings, valve train, and piston group, are described for different engine operation conditions.

#### 5.1. Resulting Valve Train Friction Losses Using the Combined Friction Analysis Approach

One of the main advantages when using the developed combined approach to analyse the friction losses is the possibility to determine the valve train friction losses with a reduced experimental effort during the conducted friction tests at the motored engine test rig. Therefore, the extended valve train friction losses are obtained using the measurement results of engine strip-stage 0 (see Figure 2) in combination with the calculated friction losses of the journal-bearings simulation methodology by applying Equation (2). It is important to note that the friction losses of the timing drive and the crankshaft seals are included in the valve train results when using the combined approach which are shown in Figure 30. This needs to be taken into account and attention has to be spent to not compare the results of the combined approach to the results from the experimental strip-test campaign presented in Figure 18.

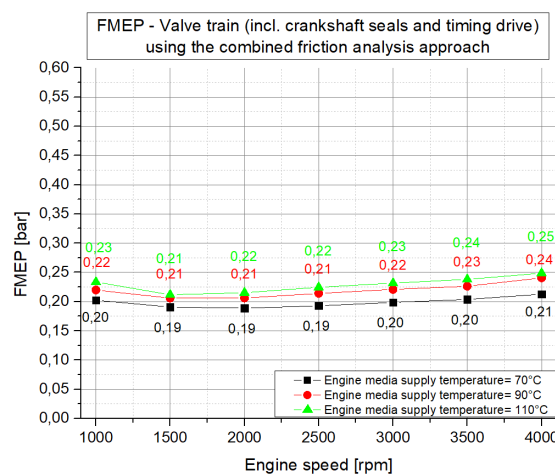


**Figure 30.** The resulting FMEP: The valve train (including the crankshaft seals and timing drive) for different engine media supply temperatures.

The resulting FMEP of the valve train (including the timing drive and crankshaft seals) shows a slight temperature dependence in the range of  $\Delta\text{FMEP} = 0.03$  bar at  $n = 1000$  rpm and  $\Delta\text{FMEP} = 0.04$  bar at  $n = 4000$  rpm between a lubricant supply temperature of  $70^\circ\text{C}$  and  $110^\circ\text{C}$ . The overall FMEP level is nearly constant over an engine speed ranging between  $\Delta\text{FMEP} = 0.02$  bar between  $n = 1000$  rpm and  $n = 4000$  rpm at the individual lubricant supply temperatures of  $70^\circ\text{C}$ ,  $90^\circ\text{C}$ , and  $110^\circ\text{C}$ . The determined valve train friction losses with timing drive and crankshaft seals included are used to calculate and allocate the subassembly friction losses according to Equation (3).

## 5.2. Subassembly-Resolved Friction Loss Distribution for the Base Engine

After the determination of the base engine friction map, the valve train friction losses using the combined approach, and the calculation of the journal-bearing friction losses, it is possible to perform the subassembly-resolved friction loss analysis of the base engine. Therefore, the basic equation of the combined approach according to Equation (3) is used to calculate the friction losses of the piston group. Figure 31 shows the results of the subassembly-resolved friction losses of the base engine for a motoring operation and different engine media supply temperatures.

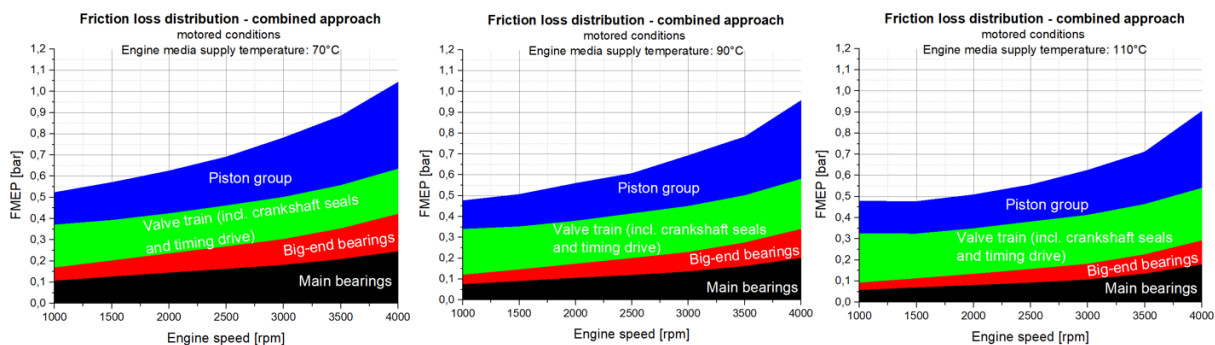


**Figure 31.** The friction loss distribution using the combined approach for different engine media supply temperatures—motored conditions.

Figure 31 shows a typical friction loss distribution for an engine speed of  $n = 4000$  rpm, where the piston group has the highest FMEP share of about 40% followed by the crankshaft journal bearings with 35% and the valve train with about 25%. In contrast, at the lowest engine speed, the FMEP share is inverted compared to the results at  $n = 4000$  rpm. At an engine speed of  $n = 1000$  rpm and an engine media supply temperature of  $110^\circ\text{C}$ , the valve train friction losses (including timing drive and crankshaft seals) are dominating with an FMEP share of up to 49% followed by the piston group with 32% and the crankshaft journal bearings with 19%. It is further interesting to note that the friction losses of the piston group and crankshaft journal bearings show a strong increase over the engine speed, whereas the friction losses of the valve train are rather constant for engine speeds higher  $n = 1500$  rpm. For engine speeds smaller than  $n = 1500$  rpm, a slight increase in the FMEP level of the valve train could be observed. It was found that the friction losses of the piston group and the crankshaft journal bearings decrease with an increasing engine media supply temperature, but the valve train friction losses showed a slight increase. A possible explanation for this result is that the friction losses of the crankshaft journal bearings and the piston group are dominated by hydrodynamic friction losses while in the subassembly valve train (including timing drive and crankshaft seals), mixed lubrication regimes occur leading to higher friction losses at increased lubricant supply temperatures and low rotational speeds.

The main advantage of applying the combined approach is that the friction loss distribution can be conducted also at a loaded engine operation. An analysis under the load operation has been done for all

investigated engine speeds according to the base engine measurement program (see Figure 13), and Figure 32 presents the results at an engine speed of  $n = 1200$  rpm for different engine media supply temperatures.

The crankshaft journal bearings and the piston group revealed an increase of the friction losses with an increasing load and a decrease of the friction losses when increasing the lubricant supply temperature. This indicates that the journal bearings and the piston group are operating mainly in a hydrodynamic lubrication regime without excessive mixed lubrication. As already described in the discussion on the motored friction loss distribution results, the valve train friction loss shares slightly increase with an increasing engine media supply temperature. The FMEP share for high load conditions at an engine media supply temperature of  $70\text{ }^{\circ}\text{C}$  is dominated by the crankshaft journal-bearings friction losses of 42% followed by the piston group with 34% and the valve train with 24%. At an engine media supply temperature of  $110\text{ }^{\circ}\text{C}$  and high load conditions, the FMEP share of the piston group is 39% followed by the crankshaft journal bearings with 31% and the valve train with 30%.

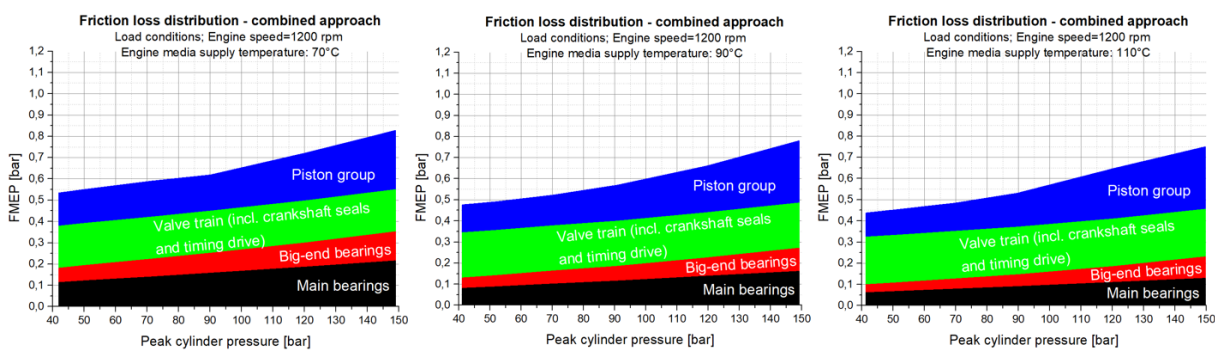


Figure 32. The friction loss distribution using the combined approach for different engine media supply temperatures—engine speed  $n = 1200$  rpm, load conditions.

Figure 33 presents FMEP results over the engine load at an engine speed of  $n = 3500$  rpm for different engine media supply temperatures of  $70\text{ }^{\circ}\text{C}$ ,  $90\text{ }^{\circ}\text{C}$ , and  $110\text{ }^{\circ}\text{C}$ .

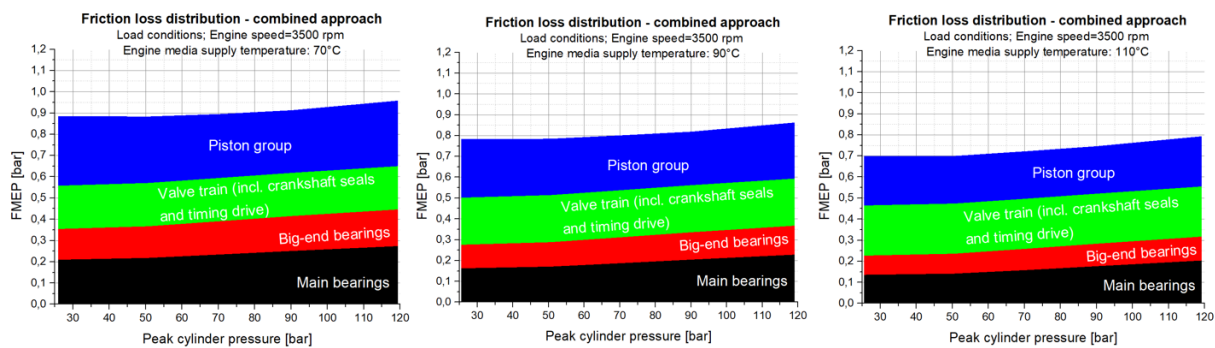


Figure 33. The friction loss distribution using the combined approach for different engine media supply temperatures—engine speed  $n = 3500$  rpm, load conditions.

As expected, the friction level for the increased engine speed of  $n = 3500$  rpm increased to FMEP = 0.9 bar at an engine media supply temperature of  $70\text{ }^{\circ}\text{C}$ . Also, in terms of the influence of acting gas forces, the friction losses of the piston group slightly decreased when the gas pressure partly compensated the acting mass forces of the piston group in low load conditions up to peak cylinder pressures of 50 bar. It was found that the friction losses of the crankshaft journal bearings as well as the piston group showed only small influences on the engine load at this engine speed level. The FMEP share at high load conditions at

an engine media supply temperature of 70 °C was dominated by the crankshaft journal-bearings friction losses of 46% followed by the piston group with 32% and the valve train with 22%. At an engine media supply temperature of 110 °C and high load conditions, the FMEP share of the crankshaft journal bearings was 40% followed by the piston group with 30% and the valve train with 30%. Summarizing, it can be said that the piston group of this engine was very efficient in terms of friction losses. Also, at very high engine loads in combination with high engine media supply temperatures, no increased FMEP could be investigated. It can also be found in the literature [41] that the piston group of this engine was friction-loss-optimized by increasing the piston clearance while lowering the piston pin offset. In addition, shorter ring heights in combination with lower tangential forces of the piston rings and friction reducing piston skirt coating was used to optimize the crank train. In another publication [16] where investigations on the friction loss potentials of the piston group were performed and analysed, it was also shown that the piston installation clearance had a marginal influence on the friction losses of the piston group among other design parameters.

## 6. Conclusions

A combined approach using measurements and a simulation to determine the friction power losses of a modern passenger-car diesel engine was used to analyse the tribological behaviour of the base engine and its subassembly crankshaft journal bearings, valve train, and piston group over the entire engine speed and load operation conditions. The approach brought together the experimental data resulting from engine friction measurements and predictive journal bearing friction loss simulations. The experimental tests were conducted using a motored engine test bed with external charging and an air recirculation system to improve the thermal boundary conditions of the piston group. The measurements were performed for different engine media supply temperatures varying between 70 °C and 110 °C to determine the tribological engine performance under changing thermal boundary conditions. In addition, a four stage strip-measurement campaign was conducted for this engine to experimentally analyse the friction losses of the valve train (including upper timing drive), lower timing drive, crankshaft seals, and crankshaft main bearings.

For the simulation part, a simulation model of the engine was created using detailed geometry, surface, and lubricant data using the approach developed by the authors that is well-documented and has a proven accuracy.

The experimental tests show that, for the entire base engine, a friction reduction potential above 20% could be realized by increasing the engine media supply temperatures from 70 °C to 110 °C. This showed that, especially for new engine modes of operation like start/stop systems and more advanced strategies like early engine stopping (e.g., at vehicle speeds below 30 km/h) using hybridization, challenges arise for the thermal management systems to keep oil temperatures at desired high levels to decrease the friction losses of the combustion engine and to maintain an optimal fuel economy. The usage of low viscosity lubricants could further improve the friction losses of the engine, especially when operating the engine at low lubricant temperatures. However, at the same time, care had to be taken regarding increased mixed lubrication in particular for low engine speeds and high lubricant supply temperatures.

The assignment of friction reduction potentials to the base engine subassemblies was possible in great detail due to the usage of the combined numerical/testing approach and the conducted extensive strip-test campaign. The main subassemblies that showed decreasing friction losses with an increasing the engine media supply temperature were the crankshaft journal bearings and the piston group. The valve train as well as the lower timing drive and crankshaft seal rings showed a rather constant level of the friction losses at engine speeds higher than 2000 rpm. While the friction torque of the crankshaft seals was slightly decreasing for engine speeds lower than 2000 rpm when increasing the lubricant supply temperatures,

the lower timing drive and the valve train showed a different behaviour. The friction torques of the lower timing drive and the valve train were increasing with an increasing lubricant supply temperature at engine speeds lower than 2000 rpm. The most significant increase could be observed at the lowest investigated engine speed of 1000 rpm. For these subassemblies, care needed to be taken regarding mixed lubrication regimes when further increasing the lubricant supply temperature and, in addition, decreasing the engine speed, resulting in low rotational shaft speeds (especially for the performance of the valve train which was working at half the speed of the crankshaft due to the required gear reduction for the timing of the engine control). Also, when considering the usage of low viscosity lubricants, the impact on the friction losses of the valve train and timing drive needed to be carefully investigated. Finally, it can be said that the piston group of the investigated diesel engine showed a very good tribological performance even under very high loads and high lubricant supply temperatures. A possible explanation for this result is that the piston group had been particularly well friction-loss-optimized by increasing the piston clearance while lowering the piston pin offset. In addition, shorter ring heights in combination with lower tangential forces of the piston rings and friction reducing the piston skirt coating had been used to optimize the crank train.

As expected for an engine that is commercially sold in the thousands, some results from the simulation were that the friction losses of the main bearings and big-end bearings were dominated by the hydrodynamic friction losses and that no severe mixed lubrication occurred for the journal bearings over the investigated engine operation range. In agreement with this result is that friction reduction potentials above 45% had been determined for the main and big-end journal bearings when increasing the lubricant supply temperatures from 70 °C to 110 °C.

The measurement of the crankshaft main bearings friction losses solely during the additionally conducted strip-test campaign enabled the verification of the utilization of the journal-bearing simulation approach in a crankshaft system for the first time. The verification between the measurement and simulation showed a good agreement of the results with a maximum deviation in the friction torque of 0.24 Nm at an engine speed of 4000 rpm and an engine media supply temperature of 90 °C. At lower engine speeds, the results were within 0.1 Nm, which confirms the good applicability of the previously developed journal-bearing simulation method.

Summarizing, the combined approach used in this work can be applied to analyse in detail the friction losses of reciprocating engines and its subassemblies crankshaft journal bearings, valve train, and piston group. This analysis can be conducted over the entire engine speed and load range for different thermal boundary conditions with a high accuracy and enables the analysis of the influence of friction reduction measures like low viscosity oils, design parameter variants of the crank train components, or comparisons between different engine concepts.

**Author Contributions:** C.K., H.A. and D.E.S. conceived and designed the experiments; C.K., H.A. and D.E.S. performed the experiments; C.K. and D.E.S. build up the simulation models; C.K. performed the calculations; All authors analysed and discussed the data; C.K. wrote the paper; D.E.S. and H.A. reviewed and edited the paper.

**Acknowledgments:** The publication was written at VIRTUAL VEHICLE Research Center in Graz and was partially funded by the COMET K2—Competence Centers for Excellent Technologies Programme of the Federal Ministry for Transport, Innovation, and Technology (bmvit); the Federal Ministry for Digital, Business, and Enterprise (bmdw); the Austrian Research Promotion Agency (FFG); the Province of Styria; and the Styrian Business Promotion Agency (SFG). Furthermore, we acknowledge the partial financial support of the Austrian Science Fund (FWF): P27806-N30.

**Conflicts of Interest:** The authors declare no conflict of interest.

Appendix A

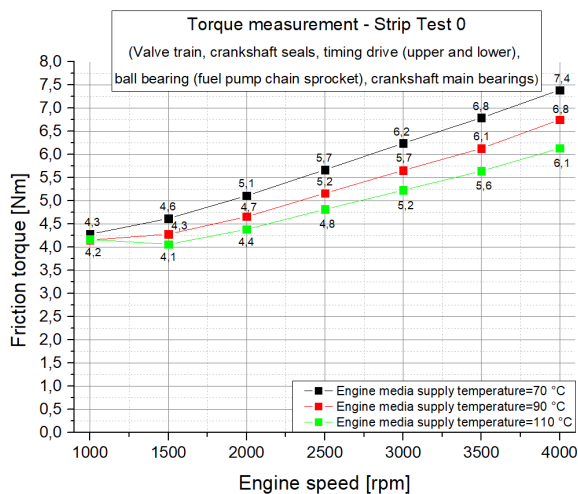


Figure A1. The resulting torque for different engine media supply temperatures: Strip-test stage 0.

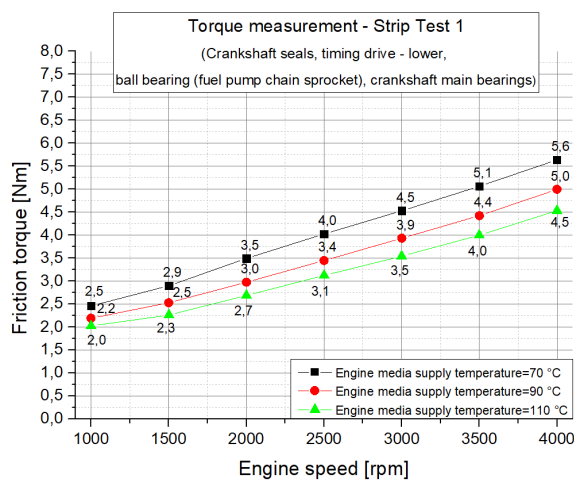


Figure A2. The resulting torque for different engine media supply temperatures: Strip-test stage 1.

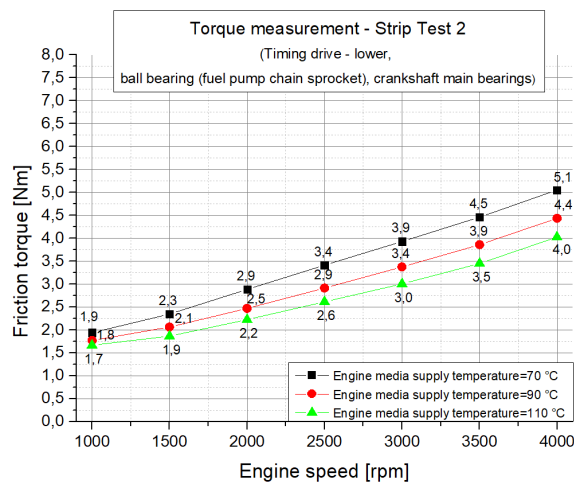


Figure A3. The resulting torque for different engine media supply temperatures: Strip-test stage 2.

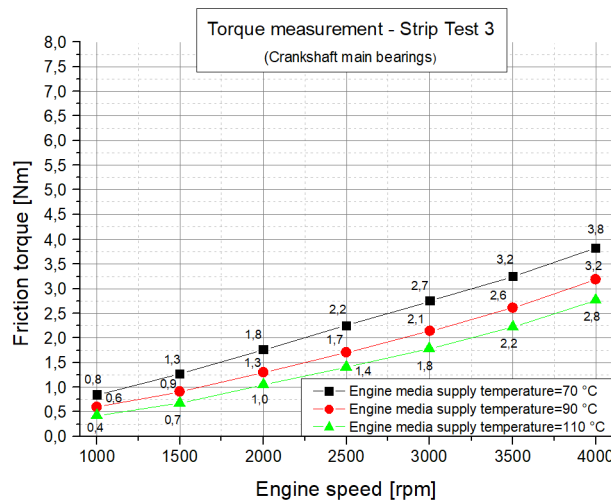


Figure A4. The resulting torque for different engine media supply temperatures: Strip-test stage 3.

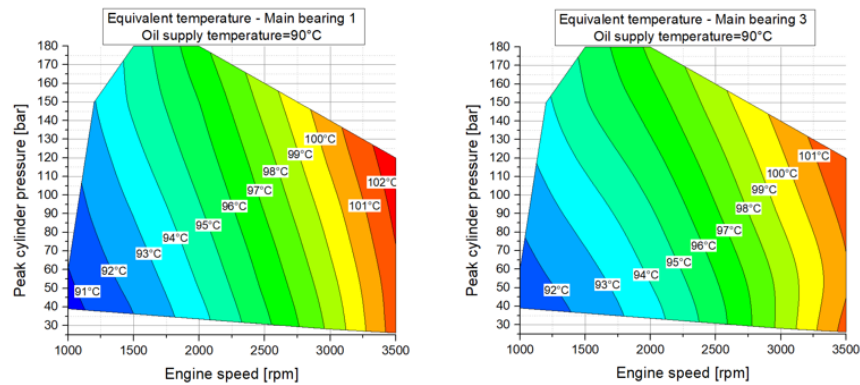


Figure A5. The equivalent temperature for the isothermal journal-bearing simulation for main bearing 1 and 3 calculated using Equation (11).

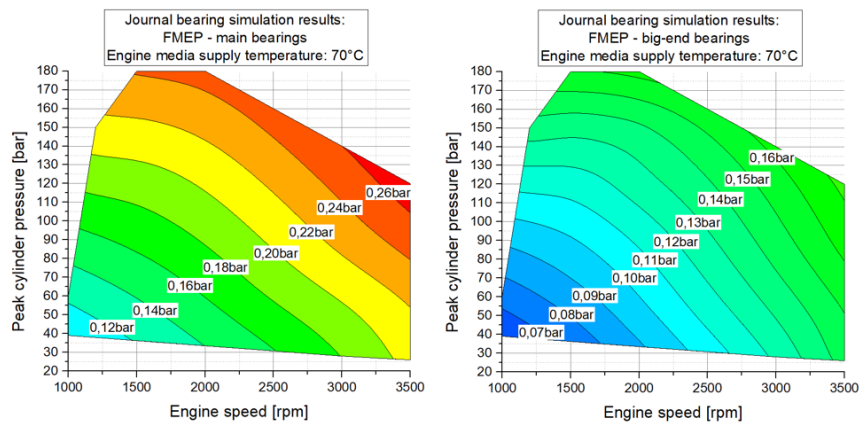
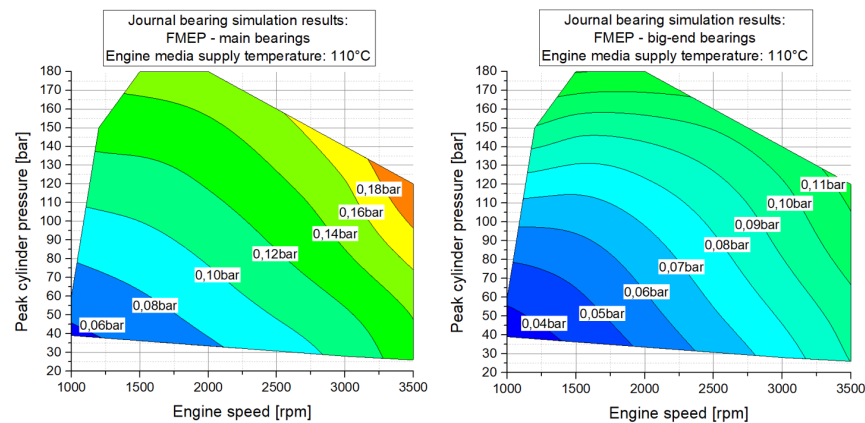
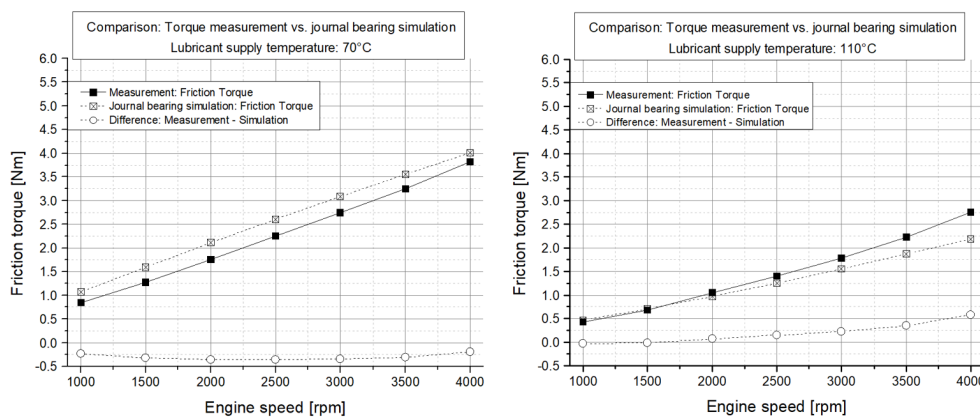


Figure A6. The resulting FMEP using the journal-bearing simulation method for main bearings and big-end bearings: lubricant supply temperature 70 °C.



**Figure A7.** The resulting FMEP using the journal-bearing simulation method for main bearings and big-end bearings: lubricant supply temperature 110 °C.



**Figure A8.** A comparison between the measurement and journal-bearing simulation for a lubricant supply temperature of 70 °C and 110 °C.

## References

1. Holmberg, K.; Andersson, P.; Erdemir, A. Global energy consumption due to friction in passenger cars. *Tribol. Int.* **2012**, *47*, 221–234. [[CrossRef](#)]
2. Schwaderlapp, M.; Dohmen, J.; Janssen, P.; Schürmann, G. Friction Reduction—The contribution of engine mechanics to fuel consumption reduction of powertrains. In Proceedings of the 22nd Aachen Colloquium Automobile and Engine Technology, Aachen, Germany, 7–9 October 2013; pp. 1273–1292.
3. Chmela, F.; Pirker, G.; Wimmer, A. Grundlagen der Motorprozessrechnung. In *Grundlagen Verbrennungsmotoren—Funktionsweise, Simulation, Messtechnik*; Merker, G.P., Teichmann, R., Eds.; Springer Fachmedien: Wiesbaden, Germany, 2014; pp. 633–707.
4. Fischer, G.D. Expertenmodell zur Berechnung der Reibungsverluste von Ottomotoren. Ph.D. Thesis, Technische Universität Darmstadt, Darmstadt, Germany, 2000.
5. Schwarzmeier, M. Der Einfluss des Arbeitsprozeßverlaufs auf den Reibmitteldruck von Dieselmotoren. Ph.D. Thesis, Technische Universität München, München, Germany, 1992.
6. Dowson, D.; Taylor, C.M.; Yang, L. Friction Modelling for Internal Combustion Engines. In *The Third Body Concept Interpretation of Tribological Phenomena*; Dowson, D., Taylor, C.M., Childs, T.H.C., Dalmaz, G., Berthier, Y., Flamand, L., Georges, J.-M., Lubrecht, A.A., Eds.; Elsevier Science B.V.: Amsterdam, The Netherlands, 1996; pp. 301–318.

7. Wichtl, R.; Schneider, R.; Grabner, P.; Eichlseder, H. Experimental and Simulative Friction Analysis of a Fired Passenger Car Diesel Engine with Focus on the Cranktrain. *SAE Int. J. Engines* **2016**, *9*, 2227–2241. [[CrossRef](#)]
8. Wichtl, R.; Eichlseder, H.; Mallinger, W.; Peterek, R. Friction Investigations on the Diesel Engine in Combustion Mode A New Measuring Method. *MTZ Worldw.* **2017**, *78*, 26–31. [[CrossRef](#)]
9. Lösch, S.; Priestner, C.; Thonhauser, B.; Zieher, F.; Hick, H. Advances in Determination of Piston Group Friction Losses at High Speeds and Loads using the AVL FRISC Single-Cylinder Engine. In Proceedings of the Reibungsminimierung im Antriebsstrang, Esslingen am Neckar, Germany, 1–2 December 2015; pp. 184–202.
10. Ullmann, K. Die Reibungs- und Pumpverluste des schnelllaufenden Otto- und Dieselmotors. *ATZ-Automobiltechnische Zeitschrift* **1939**, *42*, 397–406.
11. Ullmann, K. Die mechanischen Verluste des schnelllaufenden Dieselmotors und ihre Ermittlung im Schleppversuch. *Deutsche Kraftfahrtforschung* **1939**, *34*.
12. Caruana, C.; Farrugia, M.; Sammut, G. *The Determination of Motored Engine Friction by Use of Pressurized ‘Shunt’ Pipe between Exhaust and Intake Manifolds*; SAE Technical Paper 2018-01-0121; SAE International: Warrendale, PA, USA, 2018.
13. Mauke, D.; Dolt, R.; Stadler, J.; Huttinger, K.; Bargende, M. *Methods of Measuring Friction under Motored Conditions with External Charging*; Kistler Group: Winterthur, Switzerland, 2016.
14. Allmaier, H.; Knauder, C.; Sander, D.E.; Reich, F. Combination of Measurement and Simulation to Analyse Engine Friction. *MTZ Worldw.* **2016**, *77*, 66–71. [[CrossRef](#)]
15. Allmaier, H.; Knauder, C.; Salhofer, S.; Reich, F.M.; Schalk, E.; Wagner, A. An experimental study of the load and heat influence from combustion on engine friction. *Int. J. Engine Res.* **2016**, *17*, 347–353. [[CrossRef](#)]
16. Deuss, T.; Ehnis, H.; Freier, R.; Künzel, R. Friction power measurements of a fired diesel engine piston group potentials. *MTZ Worldw.* **2010**, *71*, 20–24. [[CrossRef](#)]
17. Sander, D.E.; Knauder, C.; Allmaier, H.; Damjanovic-Le Baleur, S.; Mallet, P. Friction Reduction Tested for a Downsized Diesel Engine with Low-Viscosity Lubricants Including a Novel Polyalkylene Glycol. *Lubricants* **2017**, *5*, 9. [[CrossRef](#)]
18. Knauder, C.; Allmaier, H.; Sander, D.E.; Sams, T. Measurement of the Crankshaft Seals Friction Losses in a Modern Passenger Car Diesel Engine. *Proc. Inst. Mech. Eng. J.* **2019**, under review.
19. Sander, D.E.; Allmaier, H.; Pribsch, H.H.; Reich, F.M. Determination of friction losses in combustion engines—Combination of measurement and validated EHD journal bearing simulation. In Proceedings of the VDI-Berichte 2202, Schweinfurt, Germany, 23–24 April 2013; pp. 165–175.
20. Knauder, C.; Allmaier, H.; Salhofer, S.; Sams, T. The impact of running-in on the friction of an automotive gasoline engine and in particular on its piston assembly and valve train. *Proc. Inst. Mech. Eng. J.* **2017**, *232*, 749–756. [[CrossRef](#)]
21. Teichmann, R.; Wimmer, A.; Winklhofer, E. Verbrennungsdiagnostik. In *Grundlagen Verbrennungsmotoren—Funktionsweise, Simulation, Messtechnik*; Merker, G.P., Teichmann, R., Eds.; Springer Fachmedien: Wiesbaden, Germany, 2014; pp. 549–629.
22. Meyer, C. Reibung in hoch belasteten EHD-Wälzkontakten. Ph.D. Thesis, Gottfried Wilhelm Leibniz Universität Hannover, Hannover, Germany, 2010.
23. Allmaier, H.; Priestner, C.; Six, C.; Pribsch, H.H.; Forstner, C.; Novotny-Farkas, F. Predicting friction reliably and accurately in journal bearings—A systematic validation of simulation results with experimental measurements. *Tribol. Int.* **2011**, *44*, 1151–1160. [[CrossRef](#)]
24. Sander, D.E.; Allmaier, H.; Pribsch, H.H.; Reich, F.M.; Witt, M.; Füllenbach, T.; Skiadas, A.; Brouwer, L.; Schwarze, H. Impact of high pressure and shear thinning on journal bearing friction. *Tribol. Int.* **2015**, *81*, 29–37. [[CrossRef](#)]
25. Allmaier, H.; Priestner, C.; Reich, F.M.; Pribsch, H.H.; Novotny-Farkas, F. Predicting friction reliably and accurately in journal bearings—Extending the simulation model to TEHD. *Tribol. Int.* **2013**, *58*, 20–28. [[CrossRef](#)]
26. Sander, D.E.; Allmaier, H.; Pribsch, H.H.; Witt, M.; Skiadas, A. Simulation of journal bearing friction in severe mixed lubrication—Validation and effect of surface smoothing due to running-in. *Tribol. Int.* **2016**, *96*, 173–183. [[CrossRef](#)]

27. Sander, D.E.; Allmaier, H.; Witt, M.; Skiadas, A. Journal Bearing Friction and Wear in Start/Stop Operation. *MTZ Worldw.* **2017**, *78*, 46–51. [[CrossRef](#)]
28. Knauder, C.; Allmaier, H.; Sander, D.E.; Salhofer, S.; Reich, F.M.; Sams, T. Analysis of the journal bearing friction losses in a heavy-duty diesel engine. *Lubricants* **2015**, *3*, 142–154. [[CrossRef](#)]
29. Sander, D.E.; Allmaier, H.; Knauder, C.; Strömstedt, F. Potentials and Risks of Reducing Friction with Future Ultra-low-viscosity Engine Oils. *MTZ Worldw.* **2018**, *79*, 20–27. [[CrossRef](#)]
30. Allmaier, H.; Priestner, C.; Sander, D.E.; Reich, F.M. Friction in automotive engines. In *Tribology in Engineering*; Pihili, H., Ed.; Intech: Rijeka, Croatia, 2013; pp. 149–184.
31. Sander, D.E.; Allmaier, H.; Priebsch, H.H. Friction and Wear in Automotive Journal Bearings Operating in Today's Severe Conditions. In *Advances in Tribology*; Darji, P.H., Ed.; Intech: Rijeka, Croatia, 2016; pp. 143–172.
32. Sander, D.E. A Validated Elasto-Hydrodynamic Simulation for Journal Bearings Operating Under Severe Conditions. Ph.D. Thesis, Technische Universität Graz, Graz, Austria, 2016.
33. Offner, G. Modelling of condensed flexible bodies considering non-linear inertia effects resulting from gross motions. *Proc. Inst. Mech. Eng. Part K J. Multi-Body Dyn.* **2011**, *225*, 204–219. [[CrossRef](#)]
34. Offner, G. Friction power loss simulation of internal combustion engines considering mixed lubricated radial slider, axial slider and piston to liner contacts. *Tribol. Trans.* **2013**, *56*, 503–515. [[CrossRef](#)]
35. Allmaier, H.; Priestner, C.; Reich, F.M.; Priebsch, H.H.; Forstner, C.; Novotny-Farkas, F. Predicting friction reliably and accurately in journal bearings—The importance of extensive oil-models. *Tribol. Int.* **2012**, *48*, 93–101. [[CrossRef](#)]
36. Coy, R.C. Practical applications of lubrication models in engines. *Tribol. Int.* **1998**, *31*, 563–571. [[CrossRef](#)]
37. Vogel, H. The law of the relation between the viscosity of liquids and the temperature. *Phys. Z.* **1921**, *22*, 645–646.
38. Barus, C. Isothermals, isopiestic and isometrics relative to viscosity. *Am. J. Sci.* **1893**, *45*, 87–96. [[CrossRef](#)]
39. Cross, M.M. Rheology of non-Newtonian fluids: A new flow equation for pseudoplastic systems. *J. Colloid Sci.* **1965**, *20*, 417–437. [[CrossRef](#)]
40. Furuhashi, S.; Oya, Y.; Hikari, S. Temperature measurements of the connecting rod, piston pin and crankpin bearing of an automobile gasoline engine. *Bull. JSME* **1966**, *9*, 181–189. [[CrossRef](#)]
41. Gießauf, G. Bewertung Unterschiedlicher Reibungsrelevanter Maßnahmen beim PKW-Dieselmotor. Master's Thesis, Technische Universität Graz, Graz, Austria, 2013.



© 2019 by the authors. Licensee MDPI, Basel, Switzerland. This article is an open access article distributed under the terms and conditions of the Creative Commons Attribution (CC BY) license (<http://creativecommons.org/licenses/by/4.0/>).